Reduced obesity, diabetes and steatosis upon cinnamon and grape pomace are associated with changes in gut microbiota and markers of gut barrier

Matthias Van Hul[1], Lucie Geurts[1], Hubert Plovier[1], Céline Druart[1], Amandine Everard[1], Marcus Ståhlman[2], Moez Rhimi[3], Kleopatra Chira,[6,7], Pierre-Louis Teissedre[6,7], Nathalie M. Delzenne[1], Emmanuelle Maguin[3], Angèle Guilbot[4], Amandine Brochot[4#], Philippe Gérard[#3], Fredrik Bäckhed[#2,5], Patrice D. Cani[1*]

[1] Université catholique de Louvain, Louvain Drug Research Institute, WELBIO (Walloon Excellence in Life sciences and BIOtechnology), Metabolism and Nutrition research group, Brussels, Belgium,

[2] Wallenberg Laboratory, University of Gothenburg, Gothenburg, Sweden

[3] Micalis, INRA, AgroParisTech, Université Paris-Saclay, 78350, Jouy-en-Josas, France.

[4] Groupe PiLeJe, 75015, Paris, France.

[5] Novo Nordisk Foundation Center for Basic Metabolic Research, Section for Metabolic Receptology and Enteroendocrinology, Faculty of Health Sciences, University of Copenhagen, Copenhagen, Denmark.

[6] Univ. Bordeaux, ISVV, EA 4577 Œnologie, F-33140 Villenave d'Ornon, France

[7] INRA, ISVV, USC 1366 Œnologie, F-33140 Villenave d'Ornon, France

[#] Equally contributed to this work

*Correspondence to: Patrice.cani@uclouvain.be
Prof. Patrice D. Cani, Université catholique de Louvain, LDRI, Metabolism and Nutrition research group, Av. E. Mounier, 73 box B1.73.11, B-1200 Brussels, Belgium. Phone: +32 2 764 73 97

Running title: Cinnamon and grape extracts shape microbiota and metabolism

Abstract

Increasing evidence suggests that polyphenols have a significant potential in the prevention and treatment of risk factors associated with metabolic syndrome. The objective of this study was to assess the metabolic outcomes of two polyphenol-containing extracts from cinnamon bark (CBE) and grape pomace (GPE) on C57BL/6J mice fed a high-fat diet (HFD) for 8 weeks.

Both CBE and GPE were able to decrease fat mass gain and adipose tissue inflammation in mice fed a HFD without reducing food intake. This was associated with reduced liver steatosis and lower plasma non-esterified fatty acids levels. We also observed a beneficial effect on glucose homeostasis as evidenced by an improved glucose tolerance and a lower insulin resistance index.

These ameliorations of the overall metabolic profile were associated to a significant impact on the microbial composition, which was more profound for the GPE than for the CBE. At the genus level, *Peptococcus* were decreased in the CBE group. In the GPE treated group, several key genera that have been previously found to be linked with HFD, metabolic effects and gut barrier integrity were affected: we observed a decrease of *Desulfovibrio, Lactococcus*, whereas *Allobaculum* and *Roseburia* were increased.

In addition, the expression of several antimicrobial peptides and tight junction proteins was increased in response to both CBE and GPE supplementation, indicating an improvement of the gut barrier function.

Collectively, these data suggest that CBE and GPE can ameliorate the overall metabolic profile of mice on a high-fat diet, partly by acting on the gut microbiota.

Introduction

With more than one third of the adult population affected worldwide, obesity-associated metabolic disorders have become a major global health challenge that extends well beyond the developed world (1). Obesity is caused by a disparity between energy intake and energy expenditure, although genetic and environmental factors also influence this balance and modify metabolism (2). Obesity is associated with an excess of (white) adipose tissue mass, insulin resistance, liver fat accumulation, chronic pro-inflammatory state and major health issues that include a plethora of comorbidities, such as type 2 diabetes, cardiovascular diseases, hypertension, stroke, and certain types of cancer (3). Weight-reducing programs that recommend switching to a healthier lifestyle with reduced caloric intake and increased physical activity, although efficient, are difficult to maintain in the long term and therefore often remain unsuccessful (4). Unfortunately, available drugs are of limited efficacy and are associated with side effects (5). Plant extracts may represent an additional option in the support of weight management strategies (6).

Among these, polyphenols, a large family of compounds identified in plants, have attracted great interest because of their beneficial health effects (7). These effects are often attributed to their ability to relieve oxidative stress-induced tissue damage associated with chronic diseases via their antioxidant activity and free radical scavenging capacities. Interestingly, some polyphenols were shown to have anti-inflammatory and antimicrobial properties, thereby influencing the host gut microbiota, and eventually the inflammatory and metabolic status (8-12). In addition, we and others have demonstrated that the gut microbiota

contributes to the development of the metabolic disorders associated with obesity by modulating appetite (13, 14), energy harvest and absorption (14-16), gut motility, intestinal barrier function, inflammation (17, 18), glucose and lipid metabolism, as well as hepatic and adipose tissue fat storage (19). It was also reported that diets containing high fat levels diminish intestinal microbial diversity, often at the expense of more beneficial bacteria (20).

The aim of the present study was to determine the effects of two extracts of plants, cinnamon and grape pomace, known to be rich in polyphenols, in a mouse model of diet-induced obesity. Anti-diabetic and anti-inflammatory properties of cinnamon were reported in experimental studies (21-26) and the beneficial effects of grapes and grape by-products were documented in different aspects of the metabolic syndrome including dyslipidaemia, diabetes, hypertension, and obesity (27-29). However, only few studies have explored the impact of dietary polyphenols on the gut microbiota and intestinal barrier functions (28, 30-32), and many aspects of this interaction remain largely unknown. This assessment was therefore one of the main objectives of this study.

Materials and Methods

Extracts

The cinnamon bark extract (CBE), ChalCinn®, (3inature, Saint-Bonnet-de-Rochefort, France) was extracted from *Cinnamomum cassia*, rich in polyphenol type-A polymers (oligomeric proanthocyanidins)(21, 33).

The grape (*Vitis vinifera L.*) pomace extract (GPE) was supplied by 3iNature and sourced from Alicante from red wine cultivar in the Rhône valley. Grape pomace is a wine by-product that is characterized by high contents of phenolic

compounds due to an incomplete extraction during the winemaking process. It is a mixture of grape skins and seeds in near-equivalent amounts together with a small amount of stems (<6 %). The main polyphenols of grape pomace are anthocyanins, hydroxycinnamic acids, flavanols and flavanol glycosides (34). Extraction was performed with ethanol/water (30:70 v/v) at 85 °C and the extract was concentrated and vacuum-dried on non-extracted grape pomace. The final product thus consisted of Alicante grape pomace enriched with its own polyphenols.

Reagents and Standards

Deionized water was purified with a Milli-Q water system (Millipore, Bedford, MA, USA). HPLC grade acetonitrile, ethyl acetate, chloroform, methanol, ethanol and acetone purchased from Scharlau (Sentmenat, Barcelona, Spain). The following chemicals were obtained from Sigma Aldrich (St. Louis, MO, USA): (+)-catechin, (–)-epicatechin, B1 [(–)-epicatechin-(4β-8)-(+)-catechin], procyanidin dimer B2 [(–)-epicatechin-(4β-8)-(–)-epicatechin], cyanidin-3-O-glucoside chloride, delphinidin-3-Oglucoside chloride, malvidin-3-O-glucoside chloride, peonidin-3-O-glucoside chloride, gallic acid.

The Laboratory of Organic Chemistry and Organometallic (Université Bordeaux 1) synthesized procyanidins dimers B3 [(+)-catechin-(4α-8)-(+)-catechin], B4 [(+)-catechin-(4α-8)-(–)-epicatechin] and a trimer (C1) [(+)-catechin-(4β-8)-(+)-catechin-(4β-8)-(–)-epicatechin] (Tarascou et al., 2006).

Grape pomace extract analysis

Tannins Extraction

GPE (1 gr of dry matter) was solubilized in water/ethanol (250 mL, 95:5, v/v) and partitioned three times with chloroform (250 mL) to remove lipophilic material. The aqueous phase was then extracted three times with ethyl acetate (250 mL) to obtain two distinctive fractions: a low molecular weight procyanidin fraction (monomeric/oligomeric tannins) in the organic phase and a high weight procyanidin fraction (polymeric tannins) in the aqueous phase. These two fractions were concentrated and lyophilized.

Anthocyanins Extraction

Anthocyanin extraction was adapted from the method of Sriram et al. (1999). GPE (1 g) was extracted four times with acidified methanol (40 mL, 0.1% HCl 12N) successively for 4 h, 12 h, 4 h and 12 h. The centrifugal supernatants were combined and evaporated in vacuo at 30 °C to remove methanol; the residue was dissolved in water and lyophilized to obtain an anthocyanin-rich powder.

Total Phenolics and Tannins, Anthocyanins

Total polyphenol contents (TPC) were determined in GPE and cinnamon bark extract (CBE). Tannin and anthocyanin contents were determined only in GPE. Crude extracts were solubilized in water/ethanol (90:10, v/v; pH 3.5 with tartaric acid) at appropriate concentrations. TPC was determined by the Folin-Ciocalteu assay [Singleton et al., 1965] and the data expressed as mg of gallic acid equivalents (GAE) per g dry weight. Total tannin content was measured by acidic hydrolysis using the method of Ribereau-Gayon and Stonestreet [Ribéreau et al.,

1966]. Anthocyanin content was determined by the SO2 bleaching procedure [Ribéreau et al., 1965].

HPLC Analysis of Anthocyanins in GPE

GPE was dissolved in water/methanol solution (50:50, v/v) at a concentration of 10 mg/mL prior to UPLC-UV analyses using a Thermo-Accela HPLC system (Thermo-Fisher, San Jose, CA, USA) composed of a PDA detector, an autosampler and a quaternary 600 series pump system controlled by an Xcalibur data system. Separation was performed on a C18 Kinetex column (100 mm × 2.1 mm, 1.7 μm). The injected volume was 2 μL. The mobile phase pumped at 200 μL/min comprised a 20 min, 7%–26% gradient of acetonitrile in water with both solvents containing 5% formic acid. Eluting peaks were monitored at 520 nm. Identification of mean peaks was performed by comparison to external standards (Anthocyans monoglucosides (cyanidin-3-O-glucoside, delphinidin-3-O-glucoside, paeonidin-3-O-glucoside, malvidin-3-O-glucoside, petunidin-3-O-glucoside), acylated anthocyans (paeonidin-3-O-glucoside, malvidin-3-O-glucoside) and coumaroylated (paeonidin-3-O-glucoside, malvidin-3-O-glucoside.The data was expressed as Malvidine3-O-glucoside equivalent/g dry weight GPE. (Ky et al. ,2014).

Determination of Individual Tannins in GPE by HPLC Analysis

GPE extract was solubilized in a methanol/water solution (50:50, v/v) at appropriate concentrations and analyses of monomeric/oligomeric tannins (catechin, epicatechin, dimers B1, B2,B3,B4 ; Trimer C2) were carried out

175 according to the method of Silva et al. [Silva et al, 2012]. The data was expressed
176 as catechin equivalent/g dry weight GPE.
177
178 **Determination of Mean Degree of Polymerization (mDP) in GPE**
179 The proanthocyanidin mean degree of polymerization (mDP) was determined
180 for GPE in monomeric/oligomeric and polymeric tannin fractions by the means
181 of phloroglucinolysis [Drinkine et al., 2007]. Analyses were carried out using the
182 same method as described by Lorrain et al. [Lorrain et al., 2011].
183 The oligomeric and polymeric proanthocyanidins were depolymerised in the
184 presence of a nucleophilic agent phloroglucinol in an acidic medium. Reversed-
185 phase HPLC analysis of the products formed allows determination of the
186 structural composition of proanthocyanidins, which are characterised by the
187 nature of their constitutive extension units (released as flavan-3-ols
188 phloroglucinol adducts) and terminal units (released as flavan-3-ols). To
189 calculate the apparent mDP, the sum of all subunits (flavan-3-ol monomer and
190 phloroglucinol adducts, in mols) was divided by the sum of all flavan-3-ol
191 monomers (in mols). GPE sample was analysed with a Surveyor series
192 instrument (Thermo-Finnigan, Les Ullis, France) equipped with a 100 x 4.6 mm
193 i.d., 3.5 µm X-Terra reversed-phase C18 column (Waters) thermostated at
194 25□□C. Detection was carried out at 280 nm using a Finnigan Surveyor PDA Plus
195 detector. The mass detection was carried out using a Finnigan LCQ DECA XP MAX
196 mass spectrometer with an ESI interface, performed in positive mode with the
197 following parameters: capillary temperature 325 _C, capillary voltage 4 V,
198 nebulizer gas flow 1.75 L/min, desolvation gas flow 1 L/min, and spray voltage 5
199 kV. The solvents used were solvent A: H2O/AcOH (99:1 v/v), and B: MeOH. The

gradient consisted of 5% B during 25 min, linear gradient 5%–20% B in 20 min, then 20%–32% B in 15 min, finally 32%–100% B in 2 min. The column was washed with 100% B for 5 min and then stabilized with the initial conditions for 10 min. The injection volume was 20 µL. The flow rate was 1 mL/min.

Cinnamon bark extract analysis

Total proanthocyanidins

In CBE, total proanthocyanidin content (PAC) was determined in EP using the BL-DMAC method as previously described (Lee et al., 2009) and quantified as A-type proanthocyanidin equivalents.

Determination of essential oil in CBE

CBE was ground and submitted to steam distillation (20,0 g of dried material) for 8 h, using a Clevenger-type apparatus without hexane at a rate of 3-4 ml/min, according European Pharmacopoeia. The volatile distillates were analyzed by GC-MS. The ratio of CBE and water (acidified by 2 ml HCL 37% m/m) was 1:10. The essential oils were stored in amber vials at 4°C until analysis. The yield oil were kept frozen at temperature -20°C up to their utilization.

The essential oil were analysed on a Agilent gas chromatograph Model 7890, coupled to a Agilent MS model 5975 coupled to a computer equipped with Chemstation, equipped with a DB5 MS column (40m X 0.18mm, 0.18µm), programming from 50°C (5 min) to 300°C at 5°C/min, 5 min hold. Helium as carrier gas (1.0 ml/min); injection in split mode (1:80) ; injector, 280°C. The MS working in electron impact mode at 70 eV; electron multiplier, 1900 V; ion source temperature, 230°C ; mass spectra data were acquired in the scan mode

in *m/z* range 33-450. The essential oil is diluted in acetone: 1/100.The essential oil were analysed on a Agilent gas chromatograph Model 7890, equipped with a DB5 MS column (40m X 0,18mm, 0.18 µm), programming from 50°C (5 min) to 300°C at 5°C/min, 5 min hold. Helium as carrier gas (1.0 ml/min); injection in split mode (1:80); injector and detector temperature, 280 and 300°C respectively. The essential oil is diluted in acetone: 1/100.

Components were identified by both GC retention times and by comparison of their mass with those present in the computer data bank and published spectra. Quantification was performed by area percent, FID-response factor = 1.

Determination of coumarin content in CBE

About 3.0 g (accurately weighed to 0,0001 g) of powdered whole plant was extracted using 150 ml methanol R as solvent under reflux during 30 min. After filtration, the filtrate was adjusted to 250,0 ml with the same solvent. The sample were filtered using 0,45 µm membrane filters (Millipore). Quantification of the constituent coumarin was carried out from the calibration curves of the HPLC chromatograms using authentic compounds. Coumarin (> 98%, HPLC) purchased from Sigma (St. Louis, MO, USA) was used as an external standard.

The coumarin content was determined according to reported methods [1] by an HPLC apparatus (Hitachi) consisting of a quaternary pump, a autosampler, and a Photodiode Array Detector (PDA). Separation was carried with a C18 column (4.6 mm x 250 mm) Purospher Star VWR. The column temperature was maintained at 25°C and the mobile phase flow rate at 1.5 ml/min. The mobile phase consisted of HPLC grade solvent Acetonitrile R and 5 g/L Phosphoric acid

(22:78 V/V). Coumarin content was quantified at 275 nm against the respective external standard.

Mice

Nine-week-old male C57BL/6J mice (Janvier, Le Genest-Saint-Isle, France) were housed in pairs in specific pathogen free conditions and in controlled environment (room temperature of 23 ± 2 °C, 12 h daylight cycle) with free access to food and water. After an acclimatization period of one week, mice were randomly assigned to one of four dietary conditions (n = 14 per group). The different diets were as follow: control diet (CT) (10 kcal% fat, D12450Ji, Research Diet, New Brunswick, NJ, USA), high-fat diet (HFD) (60 kcal% fat, D12492i Research Diet), high-fat diet supplemented with 2 g cinnamon bark extract/kg (HFD-CBE) or a high-fat diet supplemented with 8.2 g grape pomace extract/kg (HFD-GPE) during 8 weeks. Body weight, food and water intake were recorded weekly. Body composition (lean and fat mass) was assessed by using 7.5MHz time domain-nuclear magnetic resonance (TD-NMR) (LF50 Minispec, Bruker, Rheinstetten, Germany). In the final week of the experiment, feces were collected for each mouse and energy content was measured by calorimetric bomb analysis (Mouse Clinical Institute, Illkirch, France).

All mouse experiments were approved by and performed in accordance with the guidelines of the local ethics committee. Housing conditions were specified by the Belgian Law of May 29, 2013, regarding the protection of laboratory animals (agreement number LA1230314).

Oral glucose tolerance test (OGTT)

After 7 weeks of treatment, an oral glucose tolerance test (OGTT) was performed as previously described (35). Briefly, 6h-fasted mice were given an oral glucose load (2 g glucose per kg body weight) and blood glucose levels were measured at different time points: 30 min before and 15, 30, 60, 90 and 120 min after oral glucose load. Blood glucose was measured with a standard glucose meter (Accu Check, Roche, Basel, Switzerland) on blood samples collected from the tip of the tail vein.

Insulin resistance index

Plasma insulin concentration was determined using an ELISA kit (Mercodia, Uppsala, Sweden) according to the manufacturer's instructions. Insulin resistance index was determined by multiplying the area under the curve of both blood glucose (-30 to 120 min) and plasma insulin (-30 and 15 min) obtained following the oral glucose tolerance test (36). Glucose-induced insulin secretion was calculated as the difference between plasma insulin levels 30 min before and 15 min after oral glucose load.

Tissue sampling

At the end of the treatment period (week 8), 9 animals from each group were anesthetized with isoflurane (Forene, Abbott, Queenborough, Kent, England) and blood was sampled from the portal and cava veins. After exsanguination, mice were killed by cervical dislocation. Subcutaneous adipose tissue depots, intestines, muscles and liver were precisely dissected, weighed and immediately immersed in liquid nitrogen followed by storage at -80°C for further analysis.

299 **Indirect calorimetry experiments**

300 The remaining mice (*n* = 5 per group) were housed individually in specialized
301 metabolic chambers (Phenomaster, TSE Systems GmbH, Bad Homburg,
302 Germany) to measure whole energy expenditure, oxygen (O_2) consumption and
303 carbon dioxide (CO_2) production, respiratory exchange ratio (RER, calculated as
304 vCO_2/vO_2), food intake and spontaneous locomotor activity (36, 37). Activity was
305 recorded using an infrared light beam-based locomotion monitoring system
306 (expressed as counts per hour). Mice were allowed 48 h acclimatization before
307 experimental measurements. After six days of measurements, mice were killed
308 and tissues were sampled as described above.

309

310 **Histological analyses**

311 Subcutaneous adipose tissue depots were fixed in 4% paraformaldehyde for 24
312 hours at room temperature. Samples were then immersed in ethanol 100 % for
313 24 hours prior to processing for paraffin embedding.

314 To determine the adipocyte tissue diameter, paraffin sections of 8 μm were
315 stained with hematoxylin and eosin.

316 Macrophage infiltration in the adipose tissue was assessed by staining them with
317 a MAC-2/galectin-3 antibody (CL8942AP, Cedarlane Laboratories, Burlington,
318 Ontario, Canada) diluted 1:500 in blocking buffer overnight, and was detected
319 with an anti-rat igG antibody (AI-4001, Vector Laboratories, Inc., Burlingame,
320 California, USA) (10 mg/ml). Immune complexes were detected by the Dako
321 Envision kit (Agilent Technologies, Santa Clara, California, USA) according to the
322 manufacturer's instructions, and briefly counterstained with haematoxylin.

323 Hepatic lipid content was visualized by using Oil red O staining.

All analyses were performed in a blinded manner by the investigator and quantified using ImageJ software (Version 1.50a, National Institutes of Health, Bethesda, Maryland, USA). At least five high-magnification fields were selected at random for each mouse. Images were obtained using a SCN400 slide scanner and Digital Image Hub software (Leica Biosystems, Wetzlar, Germany).

RNA preparation and Real-time qPCR analysis

Total RNA was prepared from tissues using TriPure reagent (Roche). Quantification and integrity analysis of total RNA were performed by analyzing 1 µl of each sample in an Agilent 2100 Bioanalyzer (Agilent RNA 6000 Nano Kit, Agilent, Santa Clara, California, USA). cDNA was prepared by reverse transcription of 1 µg total RNA using a Reverse Transcription System kit (Promega, Madison, Wisconsin, USA). Real-time PCR was performed with the CFX96 real-time PCR system and CFX Manager 3.1 software (Bio-Rad, Hercules, California, USA) using Mesa Fast qPCR (Eurogentec, Liège, Belgium) for detection according to the manufacturer's instructions. RPL19 was chosen as the housekeeping gene. All samples were performed in duplicate, and data were analyzed according to the $2^{-\Delta\Delta CT}$ method. The identity and purity of the amplified product were assessed by melting curve analysis at the end of amplification. The primer sequences for the targeted mouse genes are presented in Table 1.

Biochemical analyses

Plasma adipokines (leptin, resistin) and inflammatory markers (IL1b, IFNg, MCP1, MIP1a, PAI1) were detected by using a Bio-Plex Milliplex kit (Millipore, Billerica, Massachusetts, USA) and their concentrations were measured by using

Luminex technology (Bio-Rad Bioplex; Bio-Rad) following the manufacturer's instructions.

Plasma non-esterified fatty acids, cholesterol and triglyceride concentrations were measured using kits coupling an enzymatic reaction with spectrophotometric detection of the reaction end-products (Diasys Diagnostic and Systems, Holzheim, Germany) according to the manufacturer's instructions.

Total lipids were measured in the liver tissue after extraction in CHCl3:MeOH according to Folch et al. (38) and adapted as follows: Briefly, 100 mg of liver tissue was homogenized in 2 ml of $CHCl_3$:MeOH (2:1) using a Tissue Lyser followed by an ultrasonic homogenizer. 400 µl of 0.9% NaCl solution was added and lipids were then extracted by vigorous shaking. After centrifugation, the lipidic phase was recovered in glass tubes and dried under a stream of N_2. Glass tubes were weighed before and after lipid extraction to quantify total lipid content. The dried residue was solubilized in 1.5 to 3 ml isopropanol depending on the lipid content.

Short chain fatty acid (SCFA) measurements

Short-chain fatty acids in cecal samples were analyzed by gas–liquid chromatography as described previously (39).

Bile Acids (BA) measurements

The extraction and analysis of bile acids were performed according to a previous work (40). Briefly, bile acids from portal vein plasma were extracted by protein precipitation with 10 volumes of IS-containing methanol. After the samples were vortexed and centrifuged, the supernatant was diluted 50 times in

methanol:water (1:1). Bile acids from cecum (15-100 mg in 2 ml polypropylene tubes filled with ceramic beads) were extracted in 500µl IS-containing methanol using a TissueLyser II instrument (Retsch, Haan, Germany). The supernatant was diluted 50 times in methanol:water (1:1). Separation was performed using water and acetonitrile on a Kinetex C18 column (2.1 ×100 mm with 1.7 µm particles; Phenomenex, Torrance, California, USA). Detection was performed using a QTRAP 5500 instrument (AB Sciex, Toronto, Canada) with MRM in negative mode.

Gut microbiota analysis

The V3-V4 region was amplified from purified DNA with the primers F343 (CTTTCCCTACACGACGCTCTTCCGATCTACGGRAGGCAGCAG) and R784 (GGAGTTCAGACGTGTGCTCTTCCGATCTTACCAGGGTATCTAATCCT) using 30 amplification cycles with an annealing temperature of 65°C. The amplicon lengths were about 510 bp (the exact length varies depending on the species). Because MiSeq sequencing enables paired 250-bp reads, the ends of each read overlap and can be stitched together to generate extremely high-quality, full-length reads covering the entire V3-V4 region. Single multiplexing was performed using a home-made 6 bp index, which was added to the R784 primer during a second PCR with 12 cycles using the forward primer (AATGATACGGCGACCACCGAGATCTACACTCTTTCCCTACACGAC) and the modified reverse primer (CAAGCAGAAGACGGCATACGAGAT-index-GTGACTGGAGTTCAGACGTGT). The resulting PCR products were purified and loaded onto the Illumina MiSeq cartridge according to the manufacturer instructions. The quality of the run was checked internally using PhiX, and for

399 further analysis, each pair-end sequence was assigned to its sample using the
400 previously integrated index.
401
402 **Bioinformatics analysis**
403 Sequences were trimmed for adaptors and assembled with Flash1.6.2 (41). PCR
404 primers were removed and sequences with sequencing errors in the primers
405 were excluded (Mothur) (42). For each sample, 12000 reads were randomly
406 selected for each sample. Chimera were removed with UCHIME (43) and Mothur
407 (42) softwares. Reads were clustered into Operational Taxonomic Units (OTUs)
408 at the 97% identity level using Esprit-tree (44). A reference sequence was picked
409 for each OTU and assigned it at different taxonomic levels (from phylum to
410 species) using the Greengenes database (release 13-5) (45) and the RDP
411 classifier (46).
412
413 **Statistical analysis**
414 Mouse data are expressed as the mean ± SEM. Differences between groups were
415 assessed using non-parametric Kruskal–Wallis one-way analysis of variance
416 (ANOVA), followed by the Dunn's multiple comparison test. Variance was
417 compared using a Bartlett's test. If variances were significantly different between
418 groups, values were normalized by Log-transformation before proceeding to the
419 analysis. When only two groups were compared, a non-parametric Mann-
420 Whitney test was used. Regimen and treatment effects on community
421 compositions were assessed using permutational multivariate analysis of
422 variances (PERMANOVA) after rarefaction of all communities to even sampling
423 depths. The abundances of all families were computed by agglomerating the

OTUs assigned to those families. For each such family, Mann-Whitney test with BH correction (47) were performed to detect the combinations (treatment) that were significantly different in terms of abundance. The same procedure was applied for each genus and for each OTUs. All analyses were done using R (R Core Team, 2015, R Foundation for Statistical Computing, Vienna, Austria)

A two-way ANOVA analysis with a Bonferonni post-hoc test on repeated measurements was performed for the evolution of glycaemia and insulinemia during the OGTT. For all analyses and for each group, any exclusion decision was supported by the use of the Grubbs test for outlier detection.

Results

Polyphenol content and profile of grape and cinnamon extracts

GPE contained 82.663 ± 2.534 mg/g total phenolics as gallic acid equivalents (GAE). Total anthocyanin and tanin contents of the GPE fraction were 43.969 ± 3.497 (as cyanidin-3-O-glucoside equivalent) and 26.006 ± 1.066 (as procyanidin B2 equivalent), respectively, (Table 2). Individual anthocyanin analysis revealed that the most abundant anthocyanins present in GPE were malvidin-3-O-glucoside (21.594 ± 0.213 mg/g), peonidin-3-O-glucoside (8.687 ± 0.258 mg/g) and malvidin-3-O-(6''-p-coumaryl-glucoside) (4.624 ± 0.012 mg/g) (Table 2). The mean degree of polymerization of the proanthocyanidins in the GPE fraction was 4.2 ± 0.025 (data not shown).

CBE contained 79 mg/g of total phenolics as GAE. Proanthocyanidin A content was 90 mg/g. Coumarin and cinnamaldehyde represented 9 mg/g and 1.8 mg/g respectively.

Effects on body weight, body composition, adipose tissues and adipokines

Body weight gain and fat mass gain were both significantly greater in all high-fat diet treated groups (HFD, HFD-CBE, HFD-GPE) than in mice fed the control diet (CT) (Fig 1A, B). Compared to the HFD-group, HFD-GPE ($p = 0.03$, 2-way repeated measurements ANOVA) and -CBE groups (trend, $p = 0.1$) had a lower fat mass gain during the last 4 week of follow-up (Fig 1B, E, F) but no significant difference in body weight and lean mass gain were observed in the extract-treated groups (Fig 1A-F).

Brown and White adipose tissue depots were consistently smaller in the extract-treated groups compared to the HFD group, but there was no statistical difference (Fig 1G-I). These findings were mirrored by a trend in reduced leptin plasma levels in the HFD-GPE group ($p = 0.08$ versus HFD, Mann-Whitney test) (Fig 1J).

The weights of liver, spleen and different muscles were not affected by the different diets (data not shown).

Effects on glucose homeostasis

Both CBE and GPE treatments significantly improved glucose tolerance, as evidenced by a lower blood glucose profile compared to the untreated HFD-fed group (Fig 2A). The effect was stronger for the HFD-CBE group as evidenced by the significantly reduced area under the curve (Fig 2B).

Mice fed a HFD were hyperinsulinemic in the fasted state, as they exhibited more than two-fold higher levels of plasma insulin as compared to control mice (Fig 2C). Mice from the HFD-GPE group produced somewhat less insulin in response to oral glucose administration compared to the HFD and HFD-CBE mice without reaching statistical significance (Fig 2C) ($p = 0.07$ versus HFD, Mann-Whitney test). This result was corroborated by a decreasing trend for glucose-induced insulin secretion compared to the HFD and HFD-CBE groups ($p = 0.08$ versus HFD, non-parametric Mann-Whitney test)(Fig 2D) and a significant improvement of the insulin resistance index (Fig 2E) in the HFD-GPE treated group. This was in accordance with a smaller adipocyte size (Fig 2F-G) and a trend in lower circulating resistin levels (Fig 2H), factors that have previously been associated with insulin resistance (37). For the HFD-CBE group no difference in glucose-

induced insulin secretion could be observed but there was a trend towards an improvement of the insulin resistance index compared to the HFD group ($p = 0.06$ versus HFD, Mann-Whitney test)(Fig 2E).

Effects on energy homeostasis

The reduced fat mass gain observed in HFD-GPE mice could not be explained by any difference in energy intake (Fig 3A). On the contrary, there was a trend towards a higher mean calorie intake in HFD-GPE mice ($p = 0.08$ versus HFD, Mann-Whitney test). HFD-GPE mice also had a significantly increased amount of feces excreted compared to the other HFD groups (Fig 3B). In addition, bomb calorimetric analysis of the different groups revealed a higher energy content in the fecal material of mice supplemented with cinnamon or grape extract (Fig 3C), resulting in higher daily energy excretion in both groups, as compared to HFD (Fig 3D). There was no difference when expressing this as percentage of the food intake (Fig3E).

The basal energy expenditure, which can also affect energy balance, was calculated by measuring the O_2 consumption and the CO_2 production for each mouse (not shown). After correction for the individual lean masses, the analysis revealed a mean increase in energy expenditure for the HFD, HFD-CBE and HFD-GPE groups, as compared to the CT group, without any effect of dietary supplementation (Fig 3F-G). In addition, body temperatures were not different between all four groups (Fig 3H). The respiratory exchange rate (RER) showed a clear metabolic shift from carbohydrate to lipid oxidation in the three HFD treated groups as compared to CT mice (Fig 3I).

Spontaneous physical activity (monitored by continuously counting the number of times a mouse crossed the different light beams in the metabolic cages) was increased in HFD-GPE mice in comparison with HFD mice ($p = 0.02$ versus HFD, 2-way repeated measurement ANOVA) (Fig 3J), whereas this effect was less pronounced in HFD-CBE mice ($p = 0.18$).

Effects on nutrients absorption

To investigate the mechanism associated with reduced energy harvest, we measured different nutrient transporters in the proximal part of the intestines (jejunum) (Fig3K). Glucose transporters (Slc5a1/SGLT1, Slc2a2/GLUT2) were slightly lower in the high-fat fed group, whereas FABP1/LFABP and CD36, fatty acid binding proteins, are higher, confirming the switch from glucose consumption to lipid oxidation. Both CBE and GPE slightly increased SGLT1, but only GPE increased GLUT2 as well. LFABP was somewhat decreased by the GPE, as was CD36 by CBE. However, these changes were too subtle to achieve statistical significance.

Effects on whole-body and hepatic lipid metabolism

The management of dyslipidemia is a key element in the prevention of cardiovascular diseases in obese and diabetic patients. Therefore, we performed an analysis of circulating and liver lipids. Interestingly, circulating non-esterified fatty acids levels (NEFAs) were higher in the HFD group than in the control group and were normalized in the CBE and GPE treated groups although without reaching significance ($p = 0.06$ and 0,08 versus HFD respectively, Mann-Whitney

529 test). Cholesterol plasma levels were increased in all HFD-treated groups,
530 whereas circulating triglycerides were similar between groups (Fig 4A).
531 In the liver, HFD increased the total lipid content by about 40%. Interestingly,
532 treatment with GPE completely blunted this effect (Fig 4B). This was reflected by
533 a significant normalization of liver triglyceride levels and a similar trend for
534 cholesterol. In the HFD-CBE group, a trend for normalization was also observed
535 for total lipid content and triglycerides, while cholesterol levels remained
536 unaffected ($p = 0.06$ versus CT, $p = 0.6$ versus HFD, Mann-Whitney test). This
537 finding was confirmed by the histological analysis that revealed significantly
538 increased hepatic lipid depots in HFD mice, and smaller lipid droplets in the
539 HFD-CBE and HFD-GPE mice (Fig 4C).
540
541 **Effects on adipose tissue and systemic inflammation**
542 Diabetes and insulin resistance being frequently associated with adipose tissue
543 inflammation (17, 48, 49), we measured various macrophage infiltration
544 markers in the subcutaneous (SAT) and visceral adipose tissue (VAT) using qPCR
545 analysis (Fig 5A and 5B, respectively). Integrin alpha X (ITGAX/CD11c),
546 lipopolysaccharide binding protein (LBP) and monocyte chemoattractant
547 protein-1 (MCP1) were upregulated by HFD and were reduced by GPE in both
548 adipose tissues. CBE supplementation decreased CD11c and LBP, but not MCP1.
549 Two other macrophage markers, F4/80 and CD68, were not differently
550 expressed in any group (Fig 5A).
551 Histological analysis of the SAT stained with MAC2/Galectin-3, a marker of
552 activated macrophages, showed a 2.5-fold higher number of macrophages in the
553 HFD mice than in CT mice (Fig 5B), whereas this accumulation of macrophages

554 was markedly decreased in the HFD-CBE and HFD-GPE groups compared to the
555 HFD group, although without reaching significance (Fig 5B).
556 To evaluate systemic inflammation, we measured circulating inflammatory
557 markers in plasma (Fig 5D). We did not find a marked HFD effect for any of the
558 markers, indicating that although there is a tissue inflammatory tone, they have
559 not yet reached systemic inflammation. However, the GPE tended to be
560 systematically lower than the other groups, especially for IFNg (p = 0,02 versus
561 HFD, Mann-Whitney test).
562
563 **Effects on gut microbiota**
564 We and others have previously linked the gut microbiota with low-grade
565 inflammation and metabolic disorders associated with HFD feeding (17, 50-52).
566 The composition of the gut microbiota of mice that received HFD was
567 significantly changed compared to those fed with CT diet, with an enrichment in
568 Firmicutes and a decrease in Bacteroidetes (Fig 6A).
569 At the phylum level, no clear differences were observed in HFD-CBE mice when
570 compared to HFD. GPE treatment, however, increased the abundance of
571 Bacteroidetes at the expense of the Proteobacteria (Fig 6A). As observed in the
572 principal coordinates analysis (PCoA), HFD feeding caused a shift in microbiota
573 composition along the axis 1, explaining more that 57% of the difference
574 observed (Fig 6C). Conversely, most mice from the HFD-CBE and HFD-GPE
575 groups were separated from the untreated HFD-fed mice according to the axis 2.
576 At the operational taxonomic units (OTUs) level, this shift was modest in the
577 HFD-CBE group but more profound in the HFD-GPE group (Fig 6B). More
578 specifically, the abundance of 11 OTUs was significantly different in HFD-CBE

mice compared with HFD mice. In HFD-GPE mice, 53 OTUs were significantly modified (Fig 6B). Interestingly, the gut microbiota from extract-treated mice differed from that of the HFD mice but also from that of the CT mice, suggesting that polyphenols may have specific effects on the gut microbiota (Fig 6D).

At the family level, CBE supplementation significantly reduced the levels of *Peptococcaceae* (classified within the Firmicutes phylum) when compared to the HFD mice (Fig 6D, E). Supplementation with GPE reduced the levels of *Desulfovibrionaceae* and *Streptococcaceae*, while increasing the levels of *Prevotellaceae* and *Erysipelotrichaceae* (Fig 6D, E).

At the genus level, *Peptococcus* were decreased in the CBE group (Fig 6F). In the GPE treated group, we observed a decrease of *Desulfovibrio*, *Clostridium sensu stricto* and *Lactococcus*, whereas *Allobaculum* and *Roseburia* were increased (Fig 6F).

Effects on intestinal barrier

HFD feeding and concomitant changes in the gut microbiota are linked to alterations in the intestinal gut barrier function and in the production of antimicrobial peptides. Here we found that HFD lowered the gene expression of the antimicrobial peptide Reg3γ all along the intestinal tract (Fig 7A and data not shown for jejunum and ileum) and lowered the expression of intectin, encoding a protein involved in the turnover of intestinal mucosa, in the colon (Fig 7B) and jejunum (data not shown).

In the colon, CBE tended to increase levels of intectin (Fig 7B) ($p = 0.008$ versus HFD, Mann-Whitney test), of the antimicrobial peptides Lyz1 ($p = 0.03$) (Fig 7F) and of the tight-junction protein claudin3 ($p = 0.03$) (Fig 7E) compared to the

HFD group. Levels of the microbicidal protein Ang4 were higher in the HFD-CBE group as compared to CT mice (Fig 7G). HFD-GPE treatment normalized the levels of Reg3γ ($p = 0.02$ versus HFD, Mann-Whitney test) (Fig 7A) in the colon and significantly increased the levels of Lyz1 (Fig 7F). The tight junction protein Occludin was somewhat higher in the treated groups when compared to CT and HFD mice, but this did not reach significance (Fig 7D). ZO-1 remained unaffected along the gastro-intestinal tract for all the HFD-treated groups (Fig 7C and data not shown).

Effects on bile acids

Primary bile acids (BAs) are synthesized by the liver and may be converted into secondary BAs as a result of biotransformation by the intestinal microbiota (53). They serve many important physiological functions, including glucose and lipid metabolism (54). HFD increased total BAs concentration in cecal content ($p = 0.03$ versus CT, Mann-Whitney test) and supplementation with CBE further increased cecal content in BAs compared to the HFD group (Fig 8A), although this did not reach statistical significance. Interestingly, this effect was due solely to an increase in conjugated BAs (Fig 8B), since unconjugated BAs levels did not differ between HFD groups (Fig 8C). At the level of individual BAs, we could not pinpoint one specific BA responsible for this increase; it was rather an accumulation of small changes throughout the BA spectrum that contributed to this overall increase (Fig 8D).

In portal vein plasma, total BA concentrations tended to be reduced in untreated HFD mice as compared to CT mice, but were higher in the HFD-CBE and HFD-GPE groups than in the HFD group, reaching levels comparable to that of the CT

group (Fig 8E). The percentage of conjugated BA tended to be increased in the HFD-GPE ($p = 0.04$ versus HFD, Mann-Whitney test)(Fig 8F), whereas unconjugated BAs tended to be decreased ($p = 0.04$) (Fig 8G). Similar to the cecum, no specific BA changed in concentration in the plasma (Fig 8H).

Bile acids are synthesized via the classical pathway under control of cholesterol 7 alpha-hydroxylase (CYP7a1) and cholesterol 8 alpha-hydroxylase (CYP8a1), or via alternate pathways, such as the one under control of cholesterol 27-hydroxylase (CYP27a1) and cholesterol 7 beta-hydroxylase (CYP7b1). To determine whether our extracts could affect bile acid production, we measured the mRNA levels of the main factors controlling these pathways in the liver (Fig 9 A-F) and ileum (Fig 9 G-H). We found a clear upregulation of CYP7a1 (Fig 9A) and a modest increase of CYP27a1 (Fig 9D) for the HFD-GPE mice, suggesting an increase in bile acid production in this group.

In the liver, bile acids can activate FXR, which has been shown to activate the expression of FGF15 in the intestine (55). FGF15 functions as a metabolic hormone, but also signals through FGFR4 in hepatocytes to inhibit expression of CYP7a1 gene, thereby acting as a negative feedback loop. Interestingly FGF15 was upregulated in ileaum of the HFD and HFD-GPE groups, but not in the HFD-CBE group (Fig 9H). Suggesting an enlarged bile acid pool in these mice. Why this is not reflected in the bile acid content remains to be determined.

Discussion

Although polyphenols are not strictly required for vital body functions in humans, there is compelling clinical and epidemiological evidence that they significantly reduce the risk of chronic diseases and promote health (7, 56, 57). However, a significant proportion of the population is not consuming sufficient quantities of dietary polyphenols as a result of inadequate vegetable and fruit intake. Therefore, concentrated polyphenol extracts might be valuable dietary supplements offering an interesting additional strategy for metabolic disorders management (12, 58, 59).

In this study, we demonstrated that both cinnamon bark and grape pomace extracts are able to ameliorate the overall metabolic profile in a model of diet-induced obesity. This is evidenced by a decrease in fat mass gain and adipose tissue inflammation and by reduced hepatic lipid content, especially in the grape pomace-treated mice, which was not compensated by elevated plasma lipid concentrations. Our data are consistent with previous reports that showed moderate but significant beneficial effect of table grape extracts on adiposity, hepatic steatosis, insulin resistance and adipose tissue inflammation (28, 30, 60-63).

We also found a clear improvement of glucose homeostasis by both extracts, as evidenced by an improved glucose tolerance and lower insulin resistance index. This was associated with a marked reduction of non-esterified fatty acids (NEFAs, free fatty acids), which have previously been found to be modulators of insulin sensitivity (64). Interestingly, although improvement of insulin resistance index was achieved by both grape and cinnamon extracts, the mechanisms

behind this seem to be different. Indeed, the HFD-GPE mice needed less insulin to achieve the same overall glucose profile, while the HFD-CBE mice had similar insulin secretion as HFD treated mice, but achieved faster glucose uptake. It has been proposed that cinnamon facilitates glucose entrance into cells by inducing glucose transporter 4 (GLUT4) translocation to the plasma membrane mediated by the LKB1-AMPK signalling pathway (65, 66), whereas grapes might activate the PI3K pathway and promote insulin action by reducing serine kinase activation and cytokine signaling (67). Our data thus suggest that both extracts might be useful additives in the management of glucose homeostasis in diabetic patients, as has been proposed previously (21, 23-25, 27).

A large fraction of dietary polyphenols reaches the colon and can be metabolized by the intestinal microbiota. Moreover, polyphenols are well known to affect intestinal bacteria (10, 11). Here, we report a significant impact of our extracts on the microbial composition, which was more profound for the GPE than for the CBE. One of the genera significantly increased by the GPE is *Roseburia*. These are bacteria that were previously found to be at a low abundance in patients with type 2 diabetes and proposed to play an important role in gut health as they have anti-inflammatory effects in the gut (68-70). Interestingly, *Roseburia* are increased by prebiotics and associated with improvements in metabolic disorders (71, 72). We also found a higher abundance of *Allobaculum* (Erysipelotrichaceae). This genus has also been shown to be increased by prebiotics (73, 74) and grape extracts (28), and has been associated with improved intestinal integrity, increased Reg3γ levels in the colon and with resistance to NAFLD development (50). Moreover, Metformin and Berberine, two clinically effective drugs for the treatment of diabetes, are associated with

698 increases in *Allobaculum* abundance (75). As for *Roseburia*, the major end
699 product of *Allobaculum* fermentation is butyrate. This SCFA is of particular
700 relevance in the gut because it is rapidly taken up by enterocytes where it serves
701 as energy source (76). Conflicting data exist about the modulation of SCFA by
702 polyphenols. Some studies reported an increase in SCFA after supplementation
703 of the diet with extracts or phenolic compounds, whereas other studies showed
704 no differences (77), but cecal SCFA content was not affected by treatments in our
705 study (Fig 10A, B, D). GPE contains about 420 mg/g of fibers, which could be
706 insufficient to induce a significant change in the microbial fermentation to
707 markedly affect SCFA production. Alternatively, utilization of short-chain fatty
708 acids by the colonocytes may be more important in this group. This is supported
709 by the drastic increase of SLC5a8, a butyrate transporter, in the colon (Fig 10C).
710 As previously described, HFD feeding increased the abundance of
711 Desulfovibrionaceae (73, 78) and *Lactococcus* (79). This was completely
712 reversed with GPE. Several genera belonging to the Desulfovibrionaceae family
713 are considered opportunistic pathogens and have been linked to some
714 inflammatory diseases (80, 81). They produce endotoxins and have the capacity
715 to reduce sulphate to H_2S (82), thereby damaging the intestinal barrier (83).
716 Indeed, H_2S has been shown to disrupt energy metabolism in the gut epithelium
717 (84). This leads to cell death and ultimately results in intestinal inflammation
718 (85). As for the HFD-CBE mice, we found similar trends for *Roseburia*,
719 *Desulfovibrio* and *Lactococcus* genera as in the HFD-GPE mice, although they did
720 not reach statistical significance. While the genus *Peptococcus* was not
721 consistently increased by HFD, we observed that CBE strongly decreased its
722 level.

Previous studies have shown a strong association between the ingestion of polyphenol extracts and the species *Akkermansia municiphila*, a bacterium known to improve metabolic disorders (12, 58). However, none of the tested treatments were associated with a modulation of *A. municiphila* (data not shown). This was unexpected, as previous studies have shown an increase in abundance of *A. muciniphila* following polyphenol treatment (reviewed in (58)). In contrast, a recent study using a grape seed extract showed no changes in *A. muciniphila* (86) and it was also reported that Resveratrol, a polyphenol mainly found in grapes, berries and a wide range of fruits, decreases *A. muciniphila* in mice (87). In vitro, a pomegranate extract significantly inhibited the growth of *A. muciniphila* (88). This may suggests that polyphenols have varied prebiotic potential on *A. muciniphila*. However, there are several design differences between the studies that may have contributed to the divergent results concerning the gut microbiota composition. First, depending on the origin of the polyphenols (for example the grape terroir) and the extraction procedure the composition of the final extracts may vary significantly. Secondly, it has been shown that gut microbiota composition is affected by diet (type and amount of fat/sugar in the diet), mouse strain and age, and mouse provider (89). Thirdly, the increase of a certain bacterial species, such as *A. muciniphila,* may depend on its baseline intestinal abundance.

In accordance with our previous findings and the changes in the gut microbiota composition, the expression of several antimicrobial peptides, including Ang4 (effective against Gram-positive and Gram-negative bacteria), Reg3γ (effective against Gram-positive bacteria), and Lyz1 (mostly effective against Gram-positive bacteria) was found to be increased in response to both

748 CBE and GPE supplementation (90). In the CBE-treated group, this was
749 accompanied by a putative increase in intestinal mucosal turnover and barrier
750 integrity in the colon, as evidenced by an increase of intectin and claudin3.
751 Gut microbiota may affect metabolic parameters by influencing the bile acid pool
752 composition. Bile acids facilitate the digestion and absorption of lipids, but they
753 also act as signaling molecules by binding to FXR, contributing to the regulation
754 of various metabolic processes (91). Bile acid content tended to be increased
755 with CBE, solely due to an increase in conjugated bile acids, suggesting a
756 decrease in bile salt hydrolase (BSH) activity within the microbial community.
757 This seems to be supported by the fact that we did not find any effect on the
758 biological markers associated with the synthesis of bile acids in this group. In
759 addition, evidence has revealed that bile acids are also able to alter the gut
760 microbiota via direct and indirect antimicrobial effects (92), and promote the
761 survival of some bile acid-tolerant bacteria such as
762 some *Lactobacillus* and *Bifidobacterium* species (93). In contrast, we found
763 evidence for an increase bile acid production in GPE treated mice. However, this
764 was not translated to higher bile acid contents in caecum of plasma.
765 Taken together, our data demonstrate that polyphenols derived from grapes or
766 cinnamon can partially counter the deleterious effects of HFD and ameliorate
767 overall metabolic parameters related to adiposity, glucose homeostasis and gut
768 barrier integrity. These changes are associated with a modulation of the
769 microbiota composition and a reduction in inflammation. Interestingly, all these
770 beneficial effects resemble that of prebiotics, even though the doses used were
771 much lower than those generally required for classical prebiotics (59, 94).

Modes of action of both compounds were found to be different, indicating that polyphenols have a broad range of targets that require further investigations. Thus, although both studied extracts positively improve glucose and lipid metabolism and reinforce the gut barrier together with changes in the gut microbiota, it is currently unknown how this beneficial effects occur. The health benefits on the host may be mediated by the microbial production of bioactive polyphenol-derived metabolites and/or by the modulation of the gut microbial community itself. Phenolic analysis indicated that the most abundant anthocyanins found in our grape pomace extract were Malvidin-3-O-glucoside, and Peonidin-3-O-glucoside (Table 2). While the antibesity and antidiabetic effects of anthocyanins have been demonstrated previously (29), the mechanisms by which these effects occur are still not clear and conflicting data still remain. Whether the beneficial effects can be attributed to a specific phenolic component or a single bacteria remains to be determined.

Importantly, this study is the first reporting a change in animal gut microbes following treatment with a cinnamon extract, as well as a comprehensive phenotyping

In conclusion, our data as well as other reports strongly support the interest to use plant extracts rich in polyphenols to improve metabolic disorders associated with obesity and metabolic disorders.

Grants and funding

PDC is a research associate at FRS-FNRS (Fonds de la Recherche Scientifique), Belgium. HP and AE are research fellows at FRS-FNRS, Belgium. PDC is the recipient of grants from the FNRS, ERC Starting Grant 2013 (European Research Council, Starting grant 336452-ENIGMO), FRFS-WELBIO under grant: WELBIO-CR-2012S-02R and the Funds Baillet-Latour grant for medical research 2015. CD's researcher position is supported by a FIRST Spin-Off grant from the Walloon Region (convention 1410053).

Acknowledgments

We would like to thank A. Barrois, H. Danthinne, T. Pringels, M. Monnoye, C. Philippe and S. Boudebbouze for excellent technical assistance. We thank R-M. Goebbels for the processing of the samples prior to histological analysis. We thank E. Bourny from the Laboratoire Provençal des Plantes Aromatiques (LPPAM), Buis les Baronnies, France, for the analysis of cinnamon extract.

Conflict of interests

PileJe (Saint-Laurent-des-Autels, France) provided funding for this study to PDC, PG and EM. AB, AG are employed by PiLeJe. There are no patents or products in development to declare.

References

1. http://www.who.int/mediacentre/factsheets/fs311/en/.
2. **Bogardus C**. Missing heritability and GWAS utility. *Obesity (Silver Spring)* 17: 209-210, 2009.
3. **Pi-Sunyer X**. The medical risks of obesity. *Postgrad Med* 121: 21-33, 2009.
4. **Christian JG, Tsai AG, and Bessesen DH**. Interpreting weight losses from lifestyle modification trials: using categorical data. *Int J Obes (Lond)* 34: 207-209, 2010.
5. **Patel D**. Pharmacotherapy for the management of obesity. *Metabolism* 64: 1376-1385, 2015.
6. **Thaiss CA, Itav S, Rothschild D, Meijer M, Levy M, Moresi C, Dohnalova L, Braverman S, Rozin S, Malitsky S, Dori-Bachash M, Kuperman Y, Biton I, Gertler A, Harmelin A, Shapiro H, Halpern Z, Aharoni A, Segal E, and Elinav E**. Persistent microbiome alterations modulate the rate of post-dieting weight regain. *Nature* 2016.
7. **Del Rio D, Rodriguez-Mateos A, Spencer JP, Tognolini M, Borges G, and Crozier A**. Dietary (poly)phenolics in human health: structures, bioavailability, and evidence of protective effects against chronic diseases. *Antioxid Redox Signal* 18: 1818-1892, 2013.
8. **Chuang CC, and McIntosh MK**. Potential mechanisms by which polyphenol-rich grapes prevent obesity-mediated inflammation and metabolic diseases. *Annu Rev Nutr* 31: 155-176, 2011.
9. **Selma MV, Espin JC, and Tomas-Barberan FA**. Interaction between phenolics and gut microbiota: role in human health. *J Agric Food Chem* 57: 6485-6501, 2009.
10. **Nohynek LJ, Alakomi HL, Kahkonen MP, Heinonen M, Helander IM, Oksman-Caldentey KM, and Puupponen-Pimia RH**. Berry phenolics: antimicrobial properties and mechanisms of action against severe human pathogens. *Nutr Cancer* 54: 18-32, 2006.
11. **Puupponen-Pimia R, Nohynek L, Meier C, Kahkonen M, Heinonen M, Hopia A, and Oksman-Caldentey KM**. Antimicrobial properties of phenolic compounds from berries. *J Appl Microbiol* 90: 494-507, 2001.
12. **Anhe FF, Roy D, Pilon G, Dudonne S, Matamoros S, Varin TV, Garofalo C, Moine Q, Desjardins Y, Levy E, and Marette A**. A polyphenol-rich cranberry extract protects from diet-induced obesity, insulin resistance and intestinal inflammation in association with increased Akkermansia spp. population in the gut microbiota of mice. *Gut* 64: 872-883, 2015.
13. **Cani PD, Dewever C, and Delzenne NM**. Inulin-type fructans modulate gastrointestinal peptides involved in appetite regulation (glucagon-like peptide-1 and ghrelin) in rats. *Br J Nutr* 92: 521-526, 2004.
14. **Backhed F, Ding H, Wang T, Hooper LV, Koh GY, Nagy A, Semenkovich CF, and Gordon JI**. The gut microbiota as an environmental factor that regulates fat storage. *Proc Natl Acad Sci U S A* 101: 15718-15723, 2004.
15. **Turnbaugh PJ, Ley RE, Mahowald MA, Magrini V, Mardis ER, and Gordon JI**. An obesity-associated gut microbiome with increased capacity for energy harvest. *Nature* 444: 1027-1031, 2006.

16. **Rabot S, Membrez M, Bruneau A, Gerard P, Harach T, Moser M, Raymond F, Mansourian R, and Chou CJ**. Germ-free C57BL/6J mice are resistant to high-fat-diet-induced insulin resistance and have altered cholesterol metabolism. *FASEB J* 24: 4948-4959, 2010.
17. **Cani PD, Amar J, Iglesias MA, Poggi M, Knauf C, Bastelica D, Neyrinck AM, Fava F, Tuohy KM, Chabo C, Waget A, Delmee E, Cousin B, Sulpice T, Chamontin B, Ferrieres J, Tanti JF, Gibson GR, Casteilla L, Delzenne NM, Alessi MC, and Burcelin R**. Metabolic endotoxemia initiates obesity and insulin resistance. *Diabetes* 56: 1761-1772, 2007.
18. **Cani PD, Bibiloni R, Knauf C, Waget A, Neyrinck AM, Delzenne NM, and Burcelin R**. Changes in gut microbiota control metabolic endotoxemia-induced inflammation in high-fat diet-induced obesity and diabetes in mice. *Diabetes* 57: 1470-1481, 2008.
19. **Cani PD**. Metabolism in 2013: The gut microbiota manages host metabolism. *Nat Rev Endocrinol* 10: 74-76, 2014.
20. **Cani PD, and Everard A**. Talking microbes: When gut bacteria interact with diet and host organs. *Mol Nutr Food Res* 60: 58-66, 2016.
21. **Liu Y, Cotillard A, Vatier C, Bastard JP, Fellahi S, Stevant M, Allatif O, Langlois C, Bieuvelet S, Brochot A, Guilbot A, Clement K, and Rizkalla SW**. A Dietary Supplement Containing Cinnamon, Chromium and Carnosine Decreases Fasting Plasma Glucose and Increases Lean Mass in Overweight or Obese Pre-Diabetic Subjects: A Randomized, Placebo-Controlled Trial. *PLoS One* 10: e0138646, 2015.
22. **Qin B, Dawson H, Polansky MM, and Anderson RA**. Cinnamon extract attenuates TNF-alpha-induced intestinal lipoprotein ApoB48 overproduction by regulating inflammatory, insulin, and lipoprotein pathways in enterocytes. *Horm Metab Res* 41: 516-522, 2009.
23. **Qin B, Nagasaki M, Ren M, Bajotto G, Oshida Y, and Sato Y**. Cinnamon extract (traditional herb) potentiates in vivo insulin-regulated glucose utilization via enhancing insulin signaling in rats. *Diabetes Res Clin Pract* 62: 139-148, 2003.
24. **Qin B, Nagasaki M, Ren M, Bajotto G, Oshida Y, and Sato Y**. Cinnamon extract prevents the insulin resistance induced by a high-fructose diet. *Horm Metab Res* 36: 119-125, 2004.
25. **Ziegenfuss TN, Hofheins JE, Mendel RW, Landis J, and Anderson RA**. Effects of a water-soluble cinnamon extract on body composition and features of the metabolic syndrome in pre-diabetic men and women. *J Int Soc Sports Nutr* 3: 45-53, 2006.
26. **Ranasinghe P, Jayawardana R, Galappaththy P, Constantine GR, de Vas Gunawardana N, and Katulanda P**. Efficacy and safety of 'true' cinnamon (Cinnamomum zeylanicum) as a pharmaceutical agent in diabetes: a systematic review and meta-analysis. *Diabet Med* 29: 1480-1492, 2012.
27. **Akaberi M, and Hosseinzadeh H**. Grapes (Vitis vinifera) as a Potential Candidate for the Therapy of the Metabolic Syndrome. *Phytother Res* 30: 540-556, 2016.
28. **Collins B, Hoffman J, Martinez K, Grace M, Lila MA, Cockrell C, Nadimpalli A, Chang E, Chuang CC, Zhong W, Mackert J, Shen W, Cooney P, Hopkins R, and McIntosh M**. A polyphenol-rich fraction obtained from table grapes decreases adiposity, insulin resistance and markers of inflammation and impacts gut microbiota in high-fat-fed mice. *J Nutr Biochem* 31: 150-165, 2016.

29. **He J, and Giusti MM**. Anthocyanins: natural colorants with health-promoting properties. *Annu Rev Food Sci Technol* 1: 163-187, 2010.
30. **Baldwin J, Collins B, Wolf PG, Martinez K, Shen W, Chuang CC, Zhong W, Cooney P, Cockrell C, Chang E, Gaskins HR, and McIntosh MK**. Table grape consumption reduces adiposity and markers of hepatic lipogenesis and alters gut microbiota in butter fat-fed mice. *J Nutr Biochem* 27: 123-135, 2016.
31. **Roopchand DE, Carmody RN, Kuhn P, Moskal K, Rojas-Silva P, Turnbaugh PJ, and Raskin I**. Dietary Polyphenols Promote Growth of the Gut Bacterium Akkermansia muciniphila and Attenuate High-Fat Diet-Induced Metabolic Syndrome. *Diabetes* 64: 2847-2858, 2015.
32. **Wang H, Xue Y, Zhang H, Huang Y, Yang G, Du M, and Zhu MJ**. Dietary grape seed extract ameliorates symptoms of inflammatory bowel disease in IL10-deficient mice. *Mol Nutr Food Res* 57: 2253-2257, 2013.
33. **Anderson RA, Broadhurst CL, Polansky MM, Schmidt WF, Khan A, Flanagan VP, Schoene NW, and Graves DJ**. Isolation and characterization of polyphenol type-A polymers from cinnamon with insulin-like biological activity. *J Agric Food Chem* 52: 65-70, 2004.
34. **Kammerer D, Claus A, Carle R, and Schieber A**. Polyphenol screening of pomace from red and white grape varieties (Vitis vinifera L.) by HPLC-DAD-MS/MS. *J Agric Food Chem* 52: 4360-4367, 2004.
35. **Cani PD, Amar J, Iglesias MA, Poggi M, Knauf C, Bastelica D, Neyrinck AM, Fava F, Tuohy KM, Chabo C, Waget A, Delmee E, Cousin B, Sulpice T, Chamontin B, Ferrieres J, Tanti JF, Gibson GR, Casteilla L, Delzenne NM, Alessi MC, and Burcelin R**. Metabolic endotoxemia initiates obesity and insulin resistance. *Diabetes* 56: 1761-1772, 2007.
36. **Geurts L, Everard A, Van Hul M, Essaghir A, Duparc T, Matamoros S, Plovier H, Castel J, Denis RG, Bergiers M, Druart C, Alhouayek M, Delzenne NM, Muccioli GG, Demoulin JB, Luquet S, and Cani PD**. Adipose tissue NAPE-PLD controls fat mass development by altering the browning process and gut microbiota. *Nat Commun* 6: 6495, 2015.
37. **Everard A, Geurts L, Caesar R, Van Hul M, Matamoros S, Duparc T, Denis RG, Cochez P, Pierard F, Castel J, Bindels LB, Plovier H, Robine S, Muccioli GG, Renauld JC, Dumoutier L, Delzenne NM, Luquet S, Backhed F, and Cani PD**. Intestinal epithelial MyD88 is a sensor switching host metabolism towards obesity according to nutritional status. *Nat Commun* 5: 5648, 2014.
38. **Folch J, Lees M, and Sloane Stanley GH**. A simple method for the isolation and purification of total lipides from animal tissues. *J Biol Chem* 226: 497-509, 1957.
39. **Lan A, Bruneau A, Bensaada M, Philippe C, Bellaud P, Rabot S, and Jan G**. Increased induction of apoptosis by Propionibacterium freudenreichii TL133 in colonic mucosal crypts of human microbiota-associated rats treated with 1,2-dimethylhydrazine. *Br J Nutr* 100: 1251-1259, 2008.
40. **Tremaroli V, Karlsson F, Werling M, Stahlman M, Kovatcheva-Datchary P, Olbers T, Fandriks L, le Roux CW, Nielsen J, and Backhed F**. Roux-en-Y Gastric Bypass and Vertical Banded Gastroplasty Induce Long-Term Changes on the Human Gut Microbiome Contributing to Fat Mass Regulation. *Cell Metab* 22: 228-238, 2015.
41. **Magoc T, and Salzberg SL**. FLASH: fast length adjustment of short reads to improve genome assemblies. *Bioinformatics* 27: 2957-2963, 2011.

42. **Schloss PD, Westcott SL, Ryabin T, Hall JR, Hartmann M, Hollister EB, Lesniewski RA, Oakley BB, Parks DH, Robinson CJ, Sahl JW, Stres B, Thallinger GG, Van Horn DJ, and Weber CF**. Introducing mothur: open-source, platform-independent, community-supported software for describing and comparing microbial communities. *Appl Environ Microbiol* 75: 7537-7541, 2009.
43. **Edgar RC, Haas BJ, Clemente JC, Quince C, and Knight R**. UCHIME improves sensitivity and speed of chimera detection. *Bioinformatics* 27: 2194-2200, 2011.
44. **Sun Y, Cai Y, Huse SM, Knight R, Farmerie WG, Wang X, and Mai V**. A large-scale benchmark study of existing algorithms for taxonomy-independent microbial community analysis. *Brief Bioinform* 13: 107-121, 2011.
45. **DeSantis TZ, Hugenholtz P, Larsen N, Rojas M, Brodie EL, Keller K, Huber T, Dalevi D, Hu P, and Andersen GL**. Greengenes, a chimera-checked 16S rRNA gene database and workbench compatible with ARB. *Appl Environ Microbiol* 72: 5069-5072, 2006.
46. **Wang Q, Garrity GM, Tiedje JM, and Cole JR**. Naive Bayesian classifier for rapid assignment of rRNA sequences into the new bacterial taxonomy. *Appl Environ Microbiol* 73: 5261-5267, 2007.
47. **Hochberg Y, and Benjamini Y**. More powerful procedures for multiple significance testing. *Stat Med* 9: 811-818, 1990.
48. **Kanda H, Tateya S, Tamori Y, Kotani K, Hiasa K, Kitazawa R, Kitazawa S, Miyachi H, Maeda S, Egashira K, and Kasuga M**. MCP-1 contributes to macrophage infiltration into adipose tissue, insulin resistance, and hepatic steatosis in obesity. *J Clin Invest* 116: 1494-1505, 2006.
49. **Patsouris D, Li PP, Thapar D, Chapman J, Olefsky JM, and Neels JG**. Ablation of CD11c-positive cells normalizes insulin sensitivity in obese insulin resistant animals. *Cell Metab* 8: 301-309, 2008.
50. **Le Roy T, Llopis M, Lepage P, Bruneau A, Rabot S, Bevilacqua C, Martin P, Philippe C, Walker F, Bado A, Perlemuter G, Cassard-Doulcier AM, and Gerard P**. Intestinal microbiota determines development of non-alcoholic fatty liver disease in mice. *Gut* 62: 1787-1794, 2013.
51. **Backhed F, Manchester JK, Semenkovich CF, and Gordon JI**. Mechanisms underlying the resistance to diet-induced obesity in germ-free mice. *Proc Natl Acad Sci U S A* 104: 979-984, 2007.
52. **Cani PD, Possemiers S, Van de Wiele T, Guiot Y, Everard A, Rottier O, Geurts L, Naslain D, Neyrinck A, Lambert DM, Muccioli GG, and Delzenne NM**. Changes in gut microbiota control inflammation in obese mice through a mechanism involving GLP-2-driven improvement of gut permeability. *Gut* 58: 1091-1103, 2009.
53. **Gerard P**. Metabolism of cholesterol and bile acids by the gut microbiota. *Pathogens* 3: 14-24, 2013.
54. **Sayin SI, Wahlstrom A, Felin J, Jantti S, Marschall HU, Bamberg K, Angelin B, Hyotylainen T, Oresic M, and Backhed F**. Gut microbiota regulates bile acid metabolism by reducing the levels of tauro-beta-muricholic acid, a naturally occurring FXR antagonist. *Cell Metab* 17: 225-235, 2013.
55. **Inagaki T, Choi M, Moschetta A, Peng L, Cummins CL, McDonald JG, Luo G, Jones SA, Goodwin B, Richardson JA, Gerard RD, Repa JJ, Mangelsdorf DJ, and Kliewer SA**. Fibroblast growth factor 15 functions as an enterohepatic signal to regulate bile acid homeostasis. *Cell Metab* 2: 217-225, 2005.

56. **Blade C, Aragones G, Arola-Arnal A, Muguerza B, Bravo FI, Salvado MJ, Arola L, and Suarez M**. Proanthocyanidins in health and disease. *Biofactors* 42: 5-12, 2016.
57. **Zhang PY**. Polyphenols in Health and Disease. *Cell Biochem Biophys* 73: 649-664, 2015.
58. **Anhe FF, Pilon G, Roy D, Desjardins Y, Levy E, and Marette A**. Triggering Akkermansia with dietary polyphenols: A new weapon to combat the metabolic syndrome? *Gut Microbes* 7: 146-153, 2016.
59. **Anhe FF, Varin TV, Le Barz M, Desjardins Y, Levy E, Roy D, and Marette A**. Gut Microbiota Dysbiosis in Obesity-Linked Metabolic Diseases and Prebiotic Potential of Polyphenol-Rich Extracts. *Curr Obes Rep* 4: 389-400, 2015.
60. **Suwannaphet W, Meeprom A, Yibchok-Anun S, and Adisakwattana S**. Preventive effect of grape seed extract against high-fructose diet-induced insulin resistance and oxidative stress in rats. *Food Chem Toxicol* 48: 1853-1857, 2010.
61. **Park SH, Park TS, and Cha YS**. Grape seed extract (Vitis vinifera) partially reverses high fat diet-induced obesity in C57BL/6J mice. *Nutr Res Pract* 2: 227-233, 2008.
62. **Terra X, Pallares V, Ardevol A, Blade C, Fernandez-Larrea J, Pujadas G, Salvado J, Arola L, and Blay M**. Modulatory effect of grape-seed procyanidins on local and systemic inflammation in diet-induced obesity rats. *J Nutr Biochem* 22: 380-387, 2011.
63. **Gourineni V, Shay NF, Chung S, Sandhu AK, and Gu L**. Muscadine grape (Vitis rotundifolia) and wine phytochemicals prevented obesity-associated metabolic complications in C57BL/6J mice. *J Agric Food Chem* 60: 7674-7681, 2012.
64. **Kahn SE, Hull RL, and Utzschneider KM**. Mechanisms linking obesity to insulin resistance and type 2 diabetes. *Nature* 444: 840-846, 2006.
65. **Absalan A, Mohiti-Ardakani J, Hadinedoushan H, and Khalili MA**. Hydro-Alcoholic Cinnamon Extract, Enhances Glucose Transporter Isotype-4 Translocation from Intracellular Compartments into the Cytoplasmic Membrane of C2C12 Myotubes. *Indian J Clin Biochem* 27: 351-356, 2012.
66. **Shen Y, Honma N, Kobayashi K, Jia LN, Hosono T, Shindo K, Ariga T, and Seki T**. Cinnamon extract enhances glucose uptake in 3T3-L1 adipocytes and C2C12 myocytes by inducing LKB1-AMP-activated protein kinase signaling. *PLoS One* 9: e87894, 2014.
67. **Yogalakshmi B, Bhuvaneswari S, Sreeja S, and Anuradha CV**. Grape seed proanthocyanidins and metformin act by different mechanisms to promote insulin signaling in rats fed high calorie diet. *J Cell Commun Signal* 8: 13-22, 2014.
68. **Aminov RI, Walker AW, Duncan SH, Harmsen HJ, Welling GW, and Flint HJ**. Molecular diversity, cultivation, and improved detection by fluorescent in situ hybridization of a dominant group of human gut bacteria related to Roseburia spp. or Eubacterium rectale. *Appl Environ Microbiol* 72: 6371-6376, 2006.
69. **Karlsson FH, Tremaroli V, Nookaew I, Bergstrom G, Behre CJ, Fagerberg B, Nielsen J, and Backhed F**. Gut metagenome in European women with normal, impaired and diabetic glucose control. *Nature* 498: 99-103, 2013.
70. **Qin J, Li Y, Cai Z, Li S, Zhu J, Zhang F, Liang S, Zhang W, Guan Y, Shen D, Peng Y, Zhang D, Jie Z, Wu W, Qin Y, Xue W, Li J, Han L, Lu D, Wu P, Dai Y, Sun X, Li Z, Tang A, Zhong S, Li X, Chen W, Xu R, Wang M, Feng Q, Gong M, Yu J,**

Zhang Y, Zhang M, Hansen T, Sanchez G, Raes J, Falony G, Okuda S, Almeida M, LeChatelier E, Renault P, Pons N, Batto JM, Zhang Z, Chen H, Yang R, Zheng W, Li S, Yang H, Wang J, Ehrlich SD, Nielsen R, Pedersen O, Kristiansen K, and Wang J. A metagenome-wide association study of gut microbiota in type 2 diabetes. *Nature* 490: 55-60, 2012.

71. **Neyrinck AM, Possemiers S, Druart C, Van de Wiele T, De Backer F, Cani PD, Larondelle Y, and Delzenne NM**. Prebiotic effects of wheat arabinoxylan related to the increase in bifidobacteria, Roseburia and Bacteroides/Prevotella in diet-induced obese mice. *PLoS One* 6: e20944, 2011.

72. **Neyrinck AM, Possemiers S, Verstraete W, De Backer F, Cani PD, and Delzenne NM**. Dietary modulation of clostridial cluster XIVa gut bacteria (Roseburia spp.) by chitin-glucan fiber improves host metabolic alterations induced by high-fat diet in mice. *J Nutr Biochem* 23: 51-59, 2012.

73. **Everard A, Lazarevic V, Gaia N, Johansson M, Stahlman M, Backhed F, Delzenne NM, Schrenzel J, Francois P, and Cani PD**. Microbiome of prebiotic-treated mice reveals novel targets involved in host response during obesity. *ISME J* 8: 2116-2130, 2014.

74. **Tachon S, Zhou J, Keenan M, Martin R, and Marco ML**. The intestinal microbiota in aged mice is modulated by dietary resistant starch and correlated with improvements in host responses. *FEMS Microbiol Ecol* 83: 299-309, 2013.

75. **Zhang X, Zhao Y, Xu J, Xue Z, Zhang M, Pang X, Zhang X, and Zhao L**. Modulation of gut microbiota by berberine and metformin during the treatment of high-fat diet-induced obesity in rats. *Sci Rep* 5: 14405, 2015.

76. **Donohoe DR, Garge N, Zhang X, Sun W, O'Connell TM, Bunger MK, and Bultman SJ**. The microbiome and butyrate regulate energy metabolism and autophagy in the mammalian colon. *Cell Metab* 13: 517-526, 2011.

77. **Mosele JI, Macia A, and Motilva MJ**. Metabolic and Microbial Modulation of the Large Intestine Ecosystem by Non-Absorbed Diet Phenolic Compounds: A Review. *Molecules* 20: 17429-17468, 2015.

78. **Zhang C, Zhang M, Pang X, Zhao Y, Wang L, and Zhao L**. Structural resilience of the gut microbiota in adult mice under high-fat dietary perturbations. *ISME J* 6: 1848-1857, 2012.

79. **Parks BW, Nam E, Org E, Kostem E, Norheim F, Hui ST, Pan C, Civelek M, Rau CD, Bennett BJ, Mehrabian M, Ursell LK, He A, Castellani LW, Zinker B, Kirby M, Drake TA, Drevon CA, Knight R, Gargalovic P, Kirchgessner T, Eskin E, and Lusis AJ**. Genetic control of obesity and gut microbiota composition in response to high-fat, high-sucrose diet in mice. *Cell Metab* 17: 141-152, 2013.

80. **Loubinoux J, Mory F, Pereira IA, and Le Faou AE**. Bacteremia caused by a strain of Desulfovibrio related to the provisionally named Desulfovibrio fairfieldensis. *J Clin Microbiol* 38: 931-934, 2000.

81. **Weglarz L, Dzierzewicz Z, Skop B, Orchel A, Parfiniewicz B, Wisniowska B, Swiatkowska L, and Wilczok T**. Desulfovibrio desulfuricans lipopolysaccharides induce endothelial cell IL-6 and IL-8 secretion and E-selectin and VCAM-1 expression. *Cell Mol Biol Lett* 8: 991-1003, 2003.

82. **Wagner M, Roger AJ, Flax JL, Brusseau GA, and Stahl DA**. Phylogeny of dissimilatory sulfite reductases supports an early origin of sulfate respiration. *J Bacteriol* 180: 2975-2982, 1998.

83. **Jakobsson HE, Rodriguez-Pineiro AM, Schutte A, Ermund A, Boysen P, Bemark M, Sommer F, Backhed F, Hansson GC, and Johansson ME**. The

composition of the gut microbiota shapes the colon mucus barrier. *EMBO Rep* 16: 164-177, 2015.
84. **Babidge W, Millard S, and Roediger W**. Sulfides impair short chain fatty acid beta-oxidation at acyl-CoA dehydrogenase level in colonocytes: implications for ulcerative colitis. *Mol Cell Biochem* 181: 117-124, 1998.
85. **Den Hond E, Hiele M, Evenepoel P, Peeters M, Ghoos Y, and Rutgeerts P**. In vivo butyrate metabolism and colonic permeability in extensive ulcerative colitis. *Gastroenterology* 115: 584-590, 1998.
86. **Liu W, Zhao S, Wang J, Shi J, Sun Y, Wang W, Ning G, Hong J, and Liu R**. Grape seed proanthocyanidin extract ameliorates inflammation and adiposity by modulating gut microbiota in high-fat diet mice. *Mol Nutr Food Res* 2017.
87. **Sung MM, Kim TT, Denou E, Soltys CM, Hamza SM, Byrne NJ, Masson G, Park H, Wishart DS, Madsen KL, Schertzer JD, and Dyck JR**. Improved Glucose Homeostasis in Obese Mice Treated With Resveratrol Is Associated With Alterations in the Gut Microbiome. *Diabetes* 66: 418-425, 2017.
88. **Henning SM, Summanen PH, Lee RP, Yang J, Finegold SM, Heber D, and Li Z**. Pomegranate ellagitannins stimulate the growth of Akkermansia muciniphila in vivo. *Anaerobe* 43: 56-60, 2017.
89. **Laukens D, Brinkman BM, Raes J, De Vos M, and Vandenabeele P**. Heterogeneity of the gut microbiome in mice: guidelines for optimizing experimental design. *FEMS Microbiol Rev* 40: 117-132, 2016.
90. **Gallo RL, and Hooper LV**. Epithelial antimicrobial defence of the skin and intestine. *Nat Rev Immunol* 12: 503-516, 2012.
91. **Wang YD, Chen WD, Moore DD, and Huang W**. FXR: a metabolic regulator and cell protector. *Cell Res* 18: 1087-1095, 2008.
92. **Begley M, Gahan CG, and Hill C**. The interaction between bacteria and bile. *FEMS Microbiol Rev* 29: 625-651, 2005.
93. **Devkota S, Wang Y, Musch MW, Leone V, Fehlner-Peach H, Nadimpalli A, Antonopoulos DA, Jabri B, and Chang EB**. Dietary-fat-induced taurocholic acid promotes pathobiont expansion and colitis in Il10-/- mice. *Nature* 487: 104-108, 2012.
94. **Bindels LB, Delzenne NM, Cani PD, and Walter J**. Towards a more comprehensive concept for prebiotics. *Nat Rev Gastroenterol Hepatol* 12: 303-310, 2015.

Figure Legends

Figure 1. Effects on body composition and adipose tissue.
8 week follow up of (A) body weight (g) with corresponding (B) fat mass (g) and (C) lean mass (g) measured by TD-NMR. (D) Body weight gain (g), (E) fat mass (g), (F) fat mass and lean mass (% of total body weight) at the end of the follow up. (G) Weight of brown adipose tissue (mg). (H) Weights of subcutaneous, epididymal and visceral adipose tissues (mg) and corresponding (I) adiposity index (%white adipose tissue/body weight). (J) Leptin plasma levels (ng/ml). Data are presented as the mean±s.e.m. '*' '**' and '#' indicate a significant difference versus HFD ($P<0.05$, $P<0.01$, $P<0.001$ respectively) as determined by a two-way ANOVA (A-C). Data with different superscript letters are significantly different ($P<0.05$) according to post-hoc one-way ANOVA (D-J).

Figure 2. Effects on Glucose homeostasis.
(A) Plasma glucose (mg/dl) profile and (B) the mean area under the curve (AUC) measured between 0 and 120 min after glucose loading (mg/dl/min). (C) Plasma insulin levels at 30 min before and 15 min after glucose loading (µg/l). (D) Glucose-induced insulin secretion, calculated as the difference between the fasting insulinemia and the insulinemia 15 min after an oral glucose load. (E) Insulin resistance index determined by multiplying the AUC of blood glucose by the AUC of insulin between 30 min before and 15 min after glucose loading. (F) Adipocyte distribution and frequency with respect to the mean diameter measured by histological analysis. (G) Mean adipocyte size (µm). (H) Resistin plasma levels measured in the vena cava (ng/ml). Data are presented as the mean±s.e.m. '*' '**' and '#' indicate a significant difference versus HFD ($P<0.05$, $P<0.01$, $P<0.001$ respectively) as determined by a two-way ANOVA (A-B). Data with different superscript letters are significantly different ($P<0.05$) according to post-hoc one-way ANOVA (B-E).

Figure 3. Effects on energy metabolism.
Energy intake: (A) mean food intake per week per mouse (kcal). Energy excretion: (B) mean amount of feces excreted per mouse in 24h (mg/24h), (C) mean energy content in feces (kcal/g) and (D) daily energy excretion as calculated using the previous values (kcal/mouse) and (E) as percentage of the food intake. (F) Energy expenditure per night per mouse (kcal/h/kg). (G) Daily energy expenditure (kCal/h/kg), (H) body temperature (°C) and (I) respiratory exchange ratio (RER). (J) Cumulative mean number of beam breaks recorded per mouse during six days. (J) qPCR analysis of glucose transporters SGLT1 and GLUT2, and of fatty acid transporters LFABP and CD36. Data are presented as the mean±s.e.m. Data with different superscript letters are significantly different ($P<0.05$) according to post-hoc one-way ANOVA (A-E). '*' and '**' indicate a

significant difference versus HFD (P<0.05 and P<0.01 respectively) as determined by a two-way ANOVA (F).

Figure 4. Effects on lipid homeostasis.
(A) Plasmatic concentrations of non-esterified fatty acids (NEFAs) (mM), cholesterol (mg/dl) and triglycerides (mg/dl). (B) Hepatic total lipid content (mg/100mg tissue), cholesterol (mmol/mg tissue) and triglycerides (mmol/mg tissue),
(C) Representative Oil Red O pictures of the liver with quantitative measurement (%). Data are presented as the mean±s.e.m. Data with different superscript letters are significantly different (P<0.05) according to post-hoc one-way ANOVA.

Figure 5. Effects on adipose tissue inflammation.
qPCR analysis of macrophage markers mRNA expression (A) in the subcutaneous and (B) the visceral adipose tissue (fold change versus CT group). (C) Representative staining of MAC2 with Hematoxylin counterstaining of subcutaneous adipose tissues and quantitative measurements of the mean number of positive cells per adipocyte counted. (D) Plasma concentrations of different inflammatory markers. Data are presented as the mean±s.e.m. Data with different superscript letters are significantly different (P<0.05) according to post-hoc one-way ANOVA.

Figure 6. Effects on gut microbiota.
Gut bacterial community analysis by 16S rRNA gene high-throughput sequencing. (A) Composition of abundant bacterial phyla identified in the microbiota of the four different groups. (B) OTUs significantly affected by grape or cinnamon supplementation under HFD. A representative 16S rRNA gene from each of the differentially expressed OTUs versus HFD mice was aligned and used to infer the phylogenetic trees shown in this figure. The color of the OTU indicates its family. (C) Principal coordinate analysis based on the weighted UniFrac analysis (PCoA + WUF) on operational taxonomic units (OTUs). Each symbol representing a single sample is colored according to the group. (D-E) Relative abundances (percentage of 16S rRNA gene sequences) of the different bacterial families in each sample among the CT, HFD, HFD-CBE, HFD-GPE groups. (F) Relative abundances (percentage of 16S rRNA sequences) of the various bacterial genera in each sample among each group of mice. Data are presented as box-plots. . '*' and '**' indicate a significant difference versus HFD (P<0.05 and P<0.01 respectively) as determined by the unpaired two-tailed Student's t-test.

Figure 7. Effects on intestinal barrier.
(A-J) qPCR analysis of various markers of the intestinal barrier integrity and anti-microbial peptides in the colon (fold change versus CT group). Data are

expressed as mean±s.e.m. Data with different superscript letters are significantly different (P<0.05) according to post-hoc one-way ANOVA.

Figure 8. Effects on bile acids.

(A) Cecal bile acid concentration (pM/mg cecal content) and percentages of (B) conjugated and (C) unconjugated bile acids. (D) Cecal bile acids content (% of total bile acids). (E) Plasma bile acid concentrations (nM) and percentages of (F) conjugated and (G) unconjugated bile acids. (H) Plasma bile acids content (% of total bile acids). (CA: cholic acid; LCA: lithocholic acid; UDCA: ursodeoxycholic acid; CDCA: chenodeoxycholic acid; DCA: deoxycholic acid; MCA: muricholic acid; T: taurine-; o: omega; a: alpha; b: beta conjugated species). Data are expressed as mean±s.e.m. Data with different superscript letters are significantly different (P<0.05) according to post-hoc one-way ANOVA.

Figure 9. Bile acid production

qPCR analysis of bile acid production/signaling markers: (A) Cyp7a1, (B) Cyp7b1, (C) Cyp8a1, (D) cyp27a1, (E) FXR, (F) FGFR4 in the liver. (G) FXR and (H) FGF15 in the ileum. Data are expressed as mean±s.e.m. Data with different superscript letters are significantly different (P<0.05) according to post-hoc one-way ANOVA.

Figure 10. Cecal short-chain fatty acids (SCFA)

Concentration of (A) Total short-chain fatty acids (SCFA) content and (B) iso-SCFA in the caecum (μmol/g cecal content). (C) mRNA levels of the butyrate transporter SLC5a8 in the colon. (D) Relative concentrations of Acetate, Butyrate and Propionate (% of total SCFA). Data are expressed as mean±s.e.m. Data with different superscript letters are significantly different (P<0.05) according to post-hoc one-way ANOVA.

Table 1

qPCR primer sequences for the targeted mouse genes.

Table 2

Concentrations of the main components of grape pomace extract and cinnamon extract.

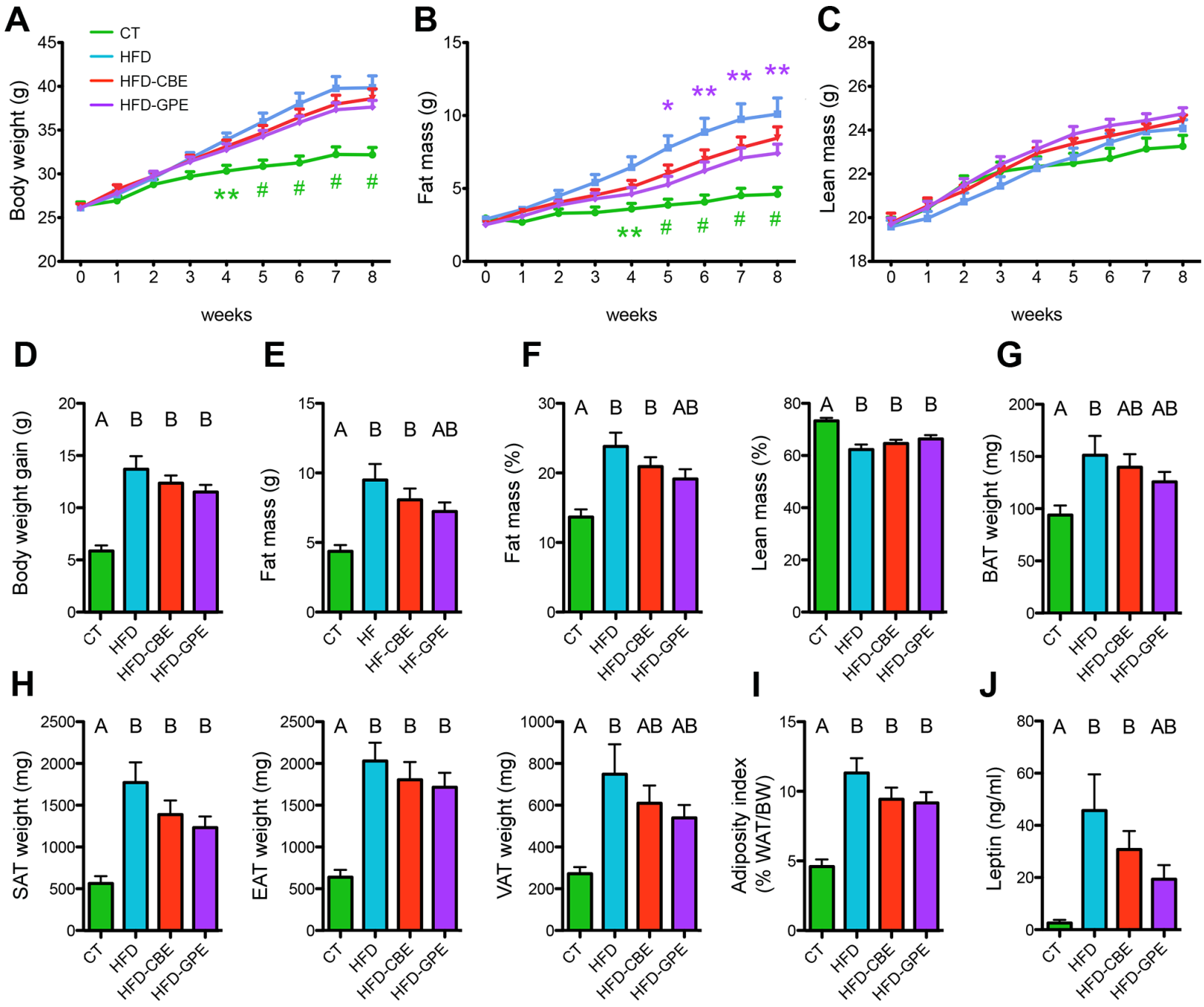

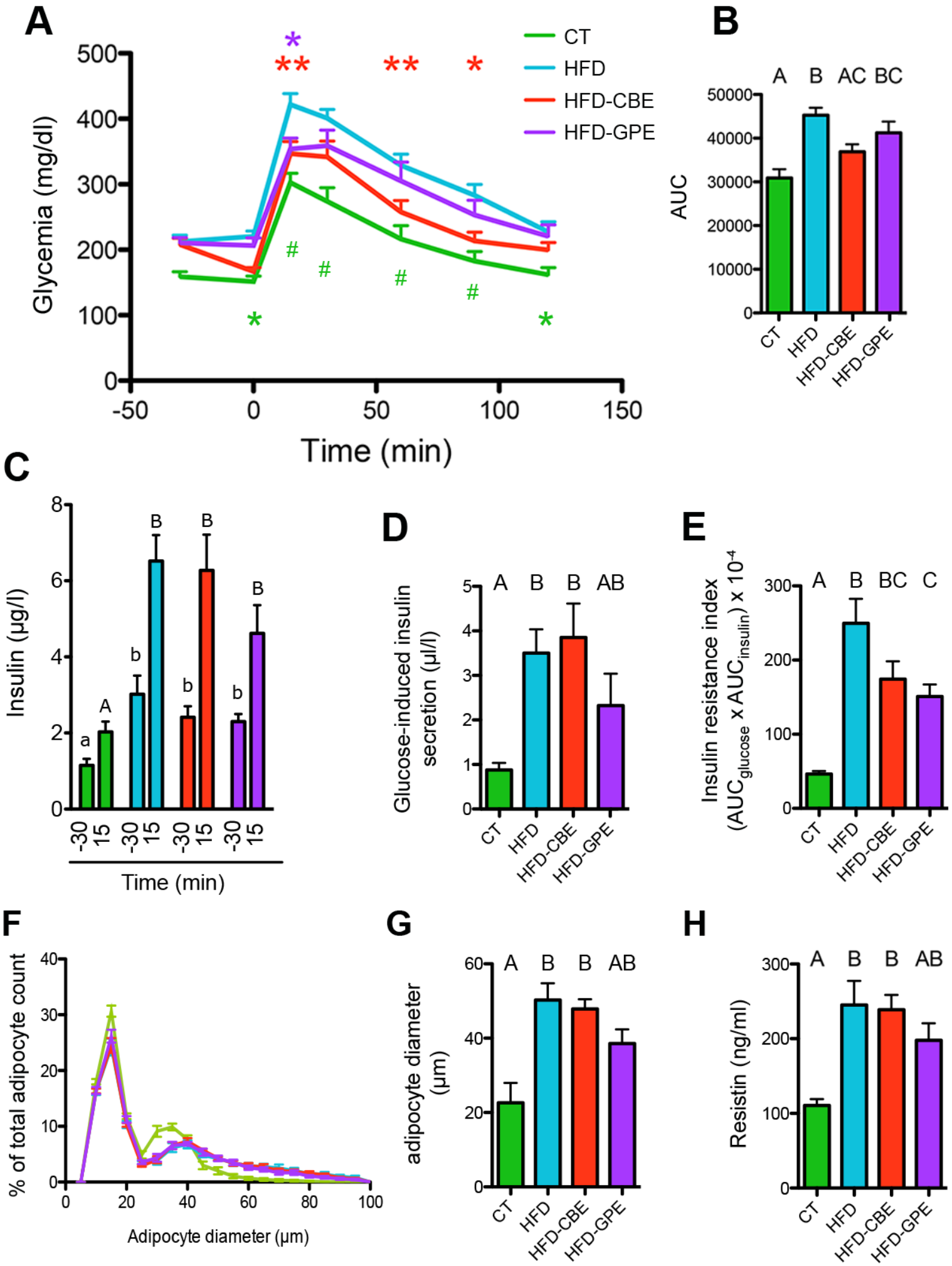

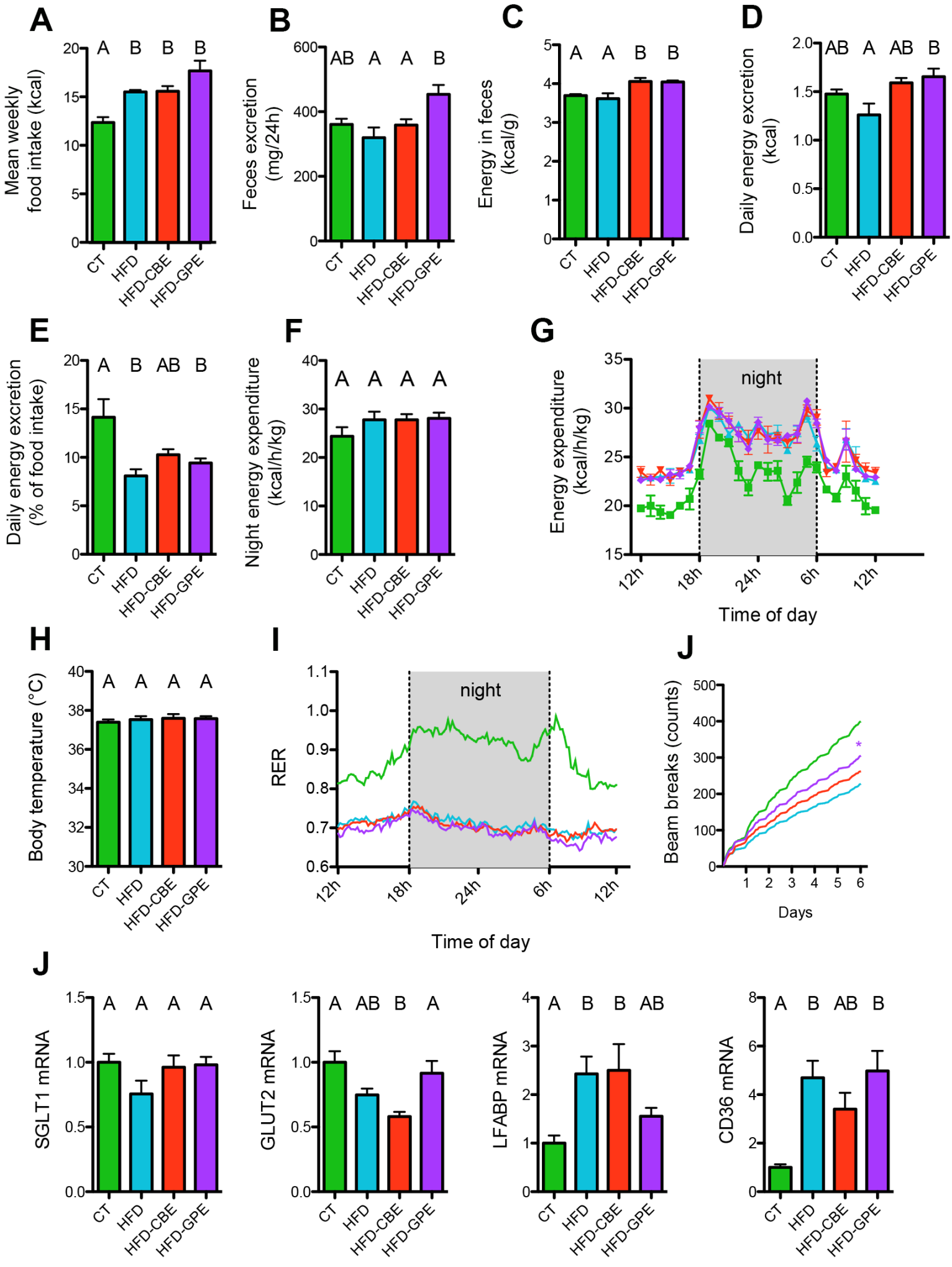

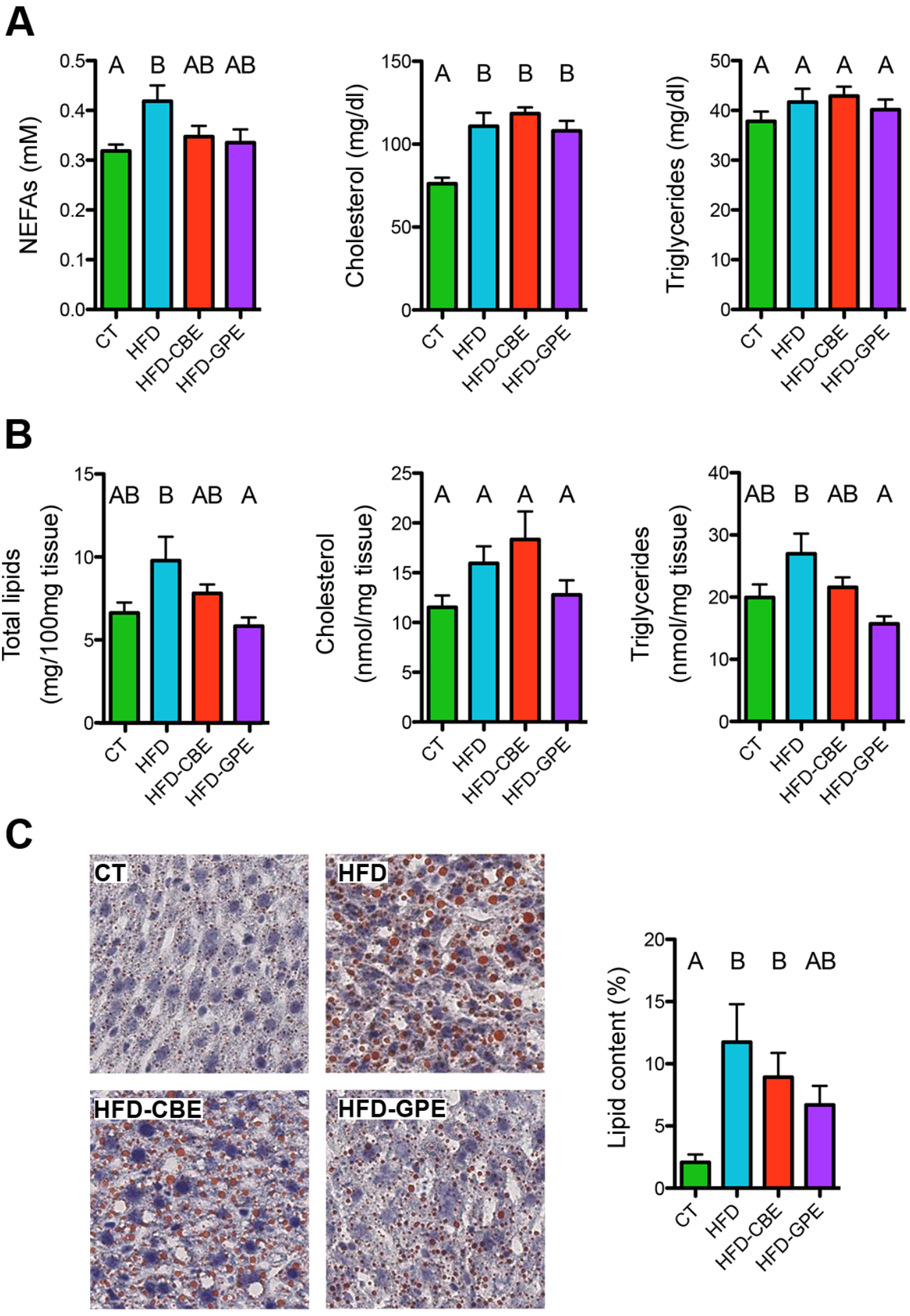

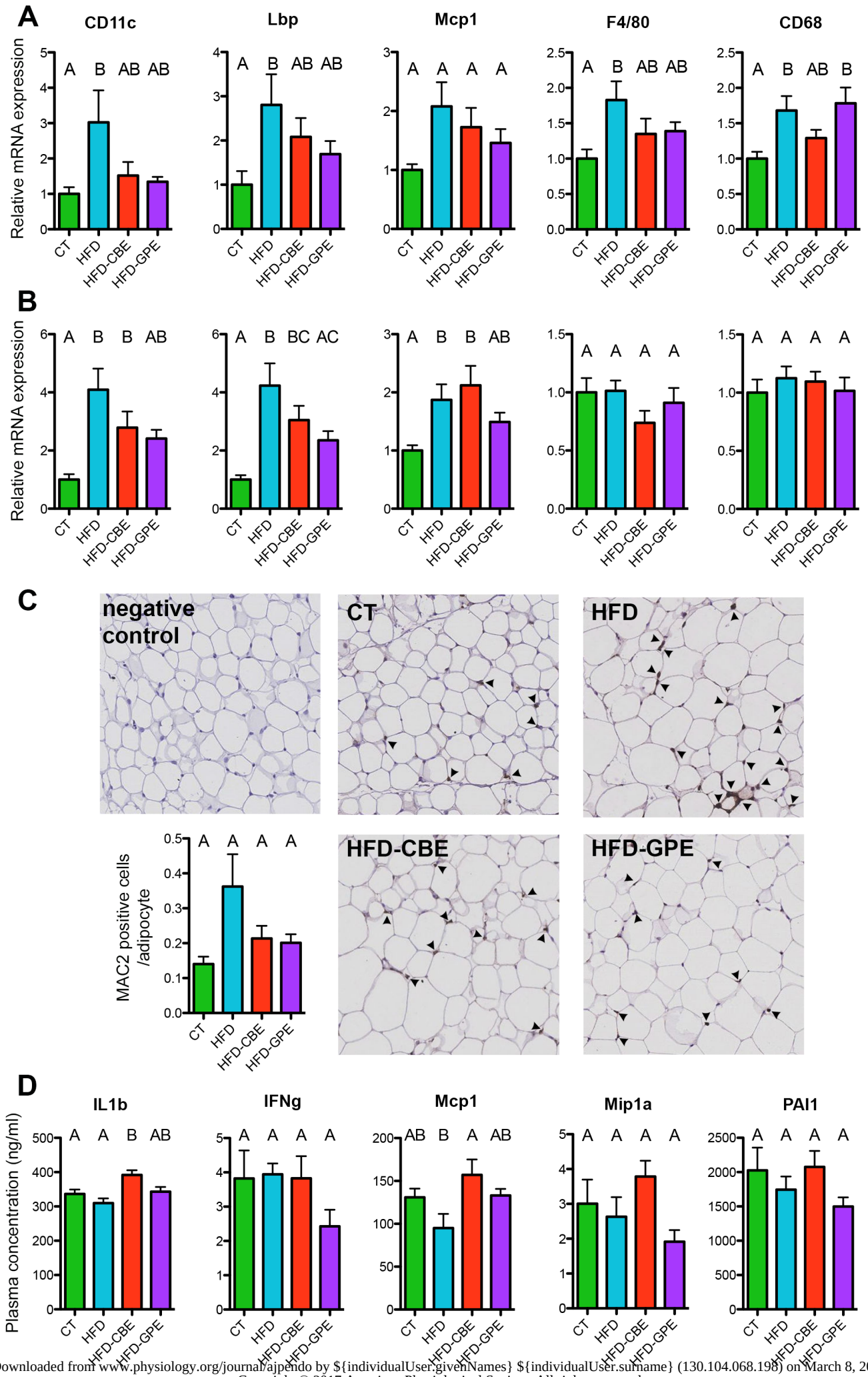

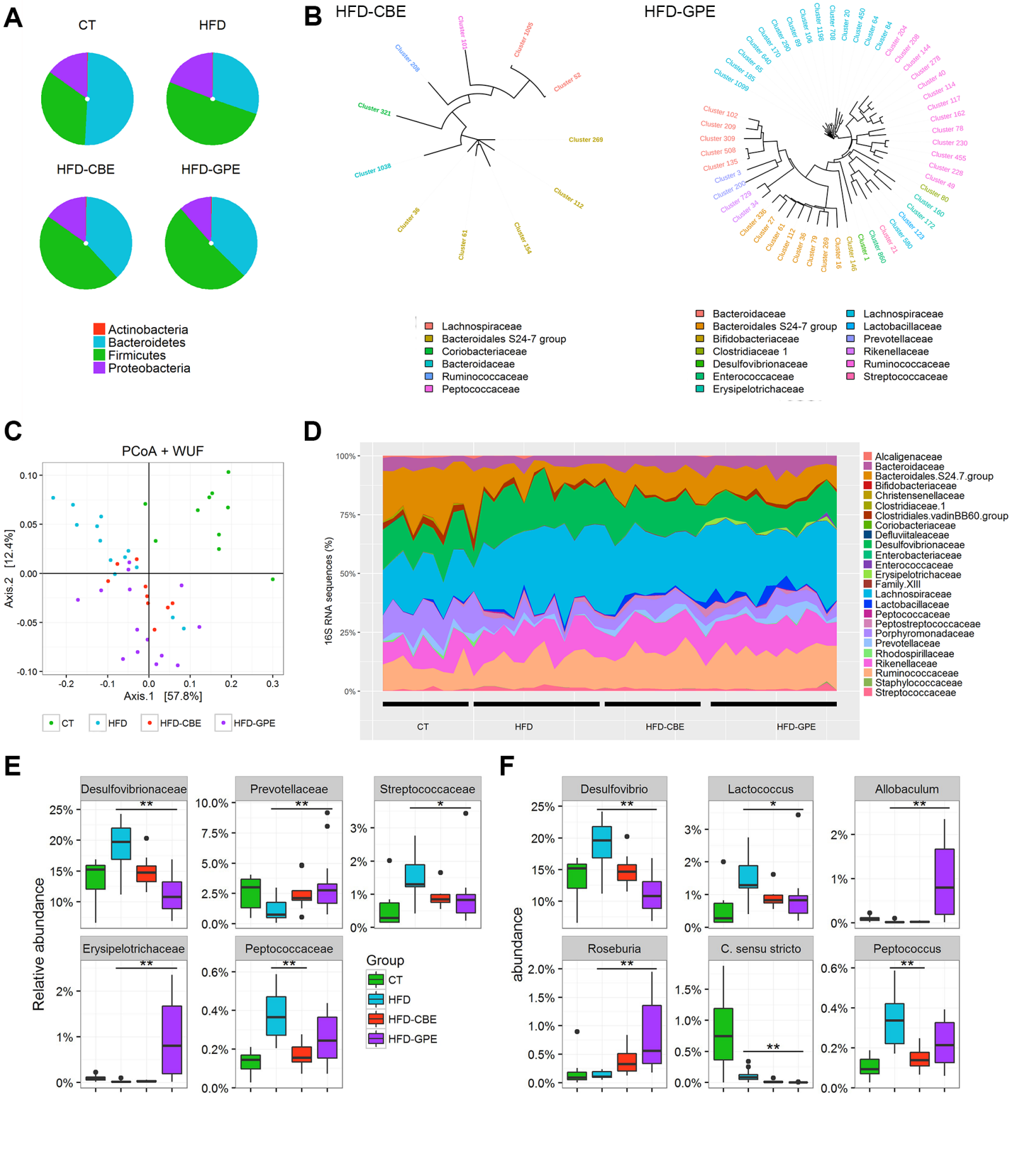

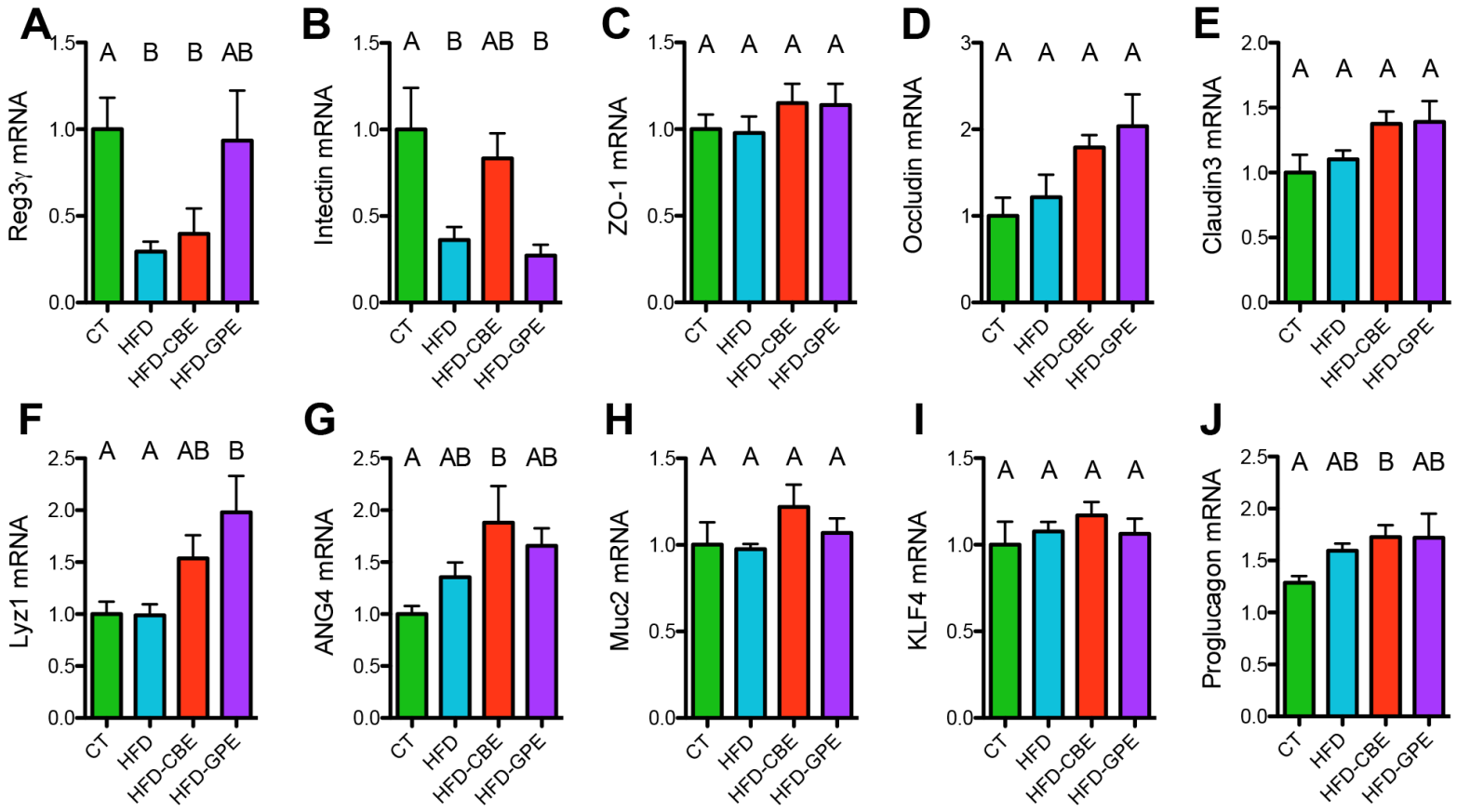

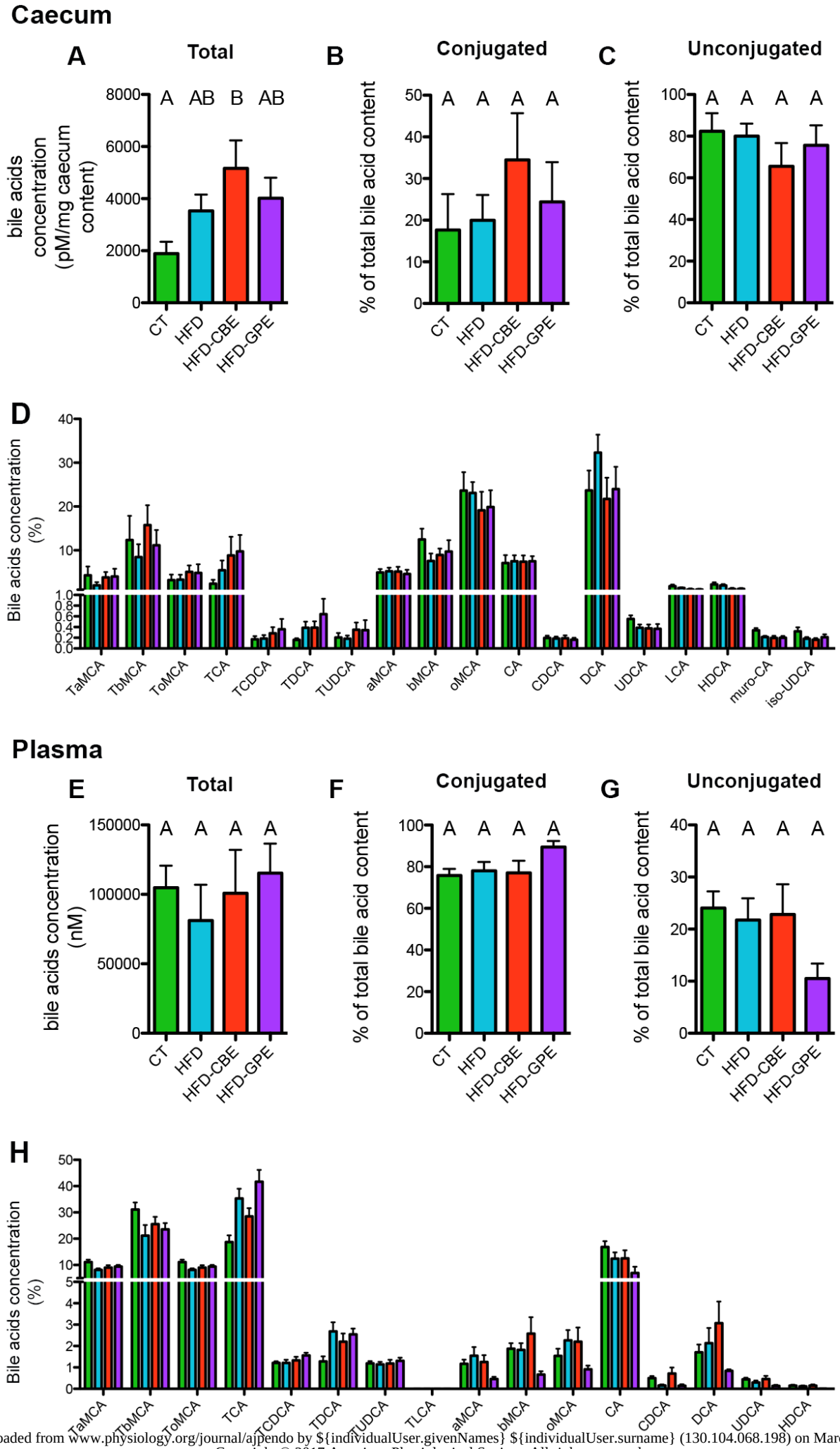

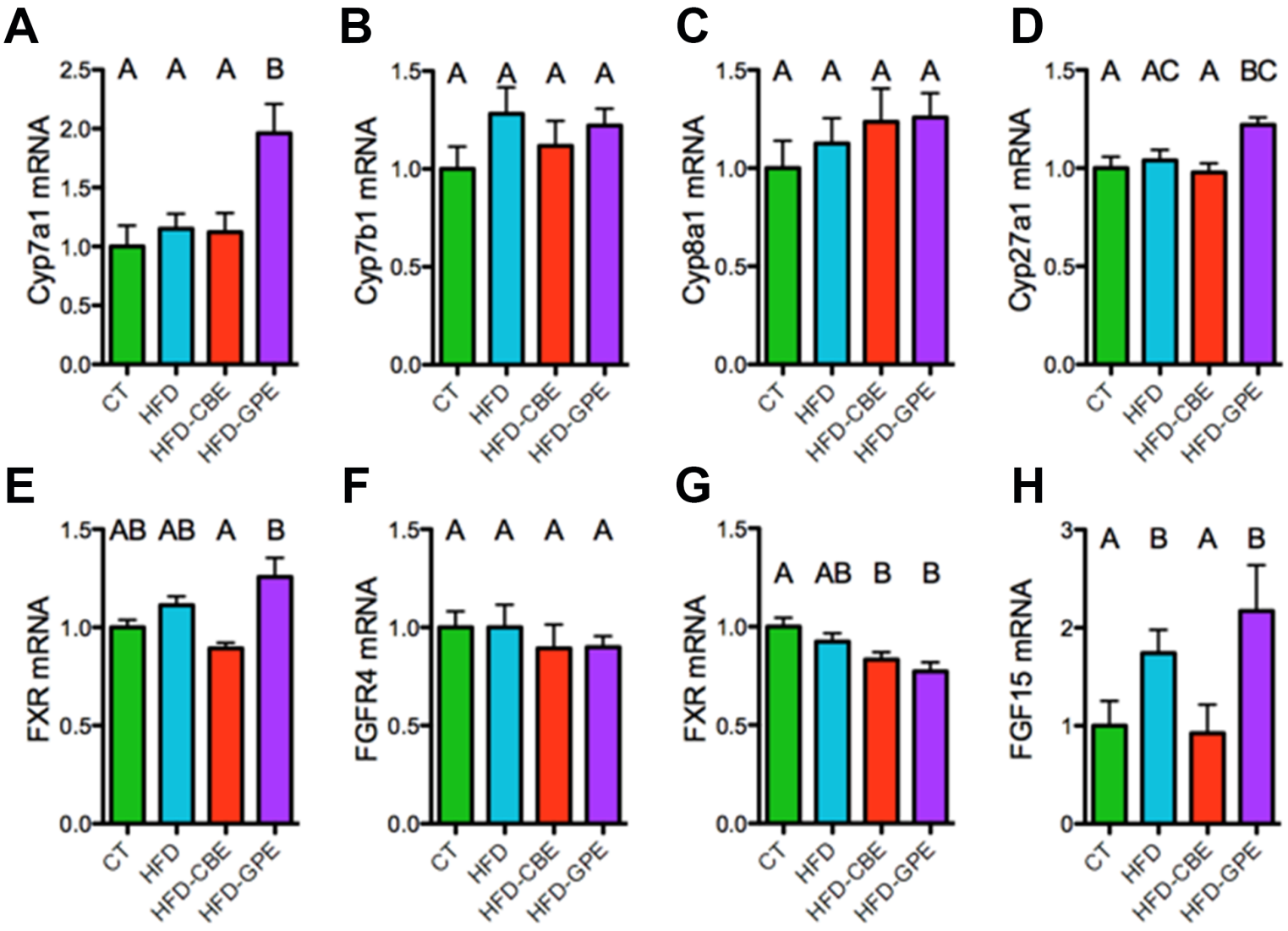

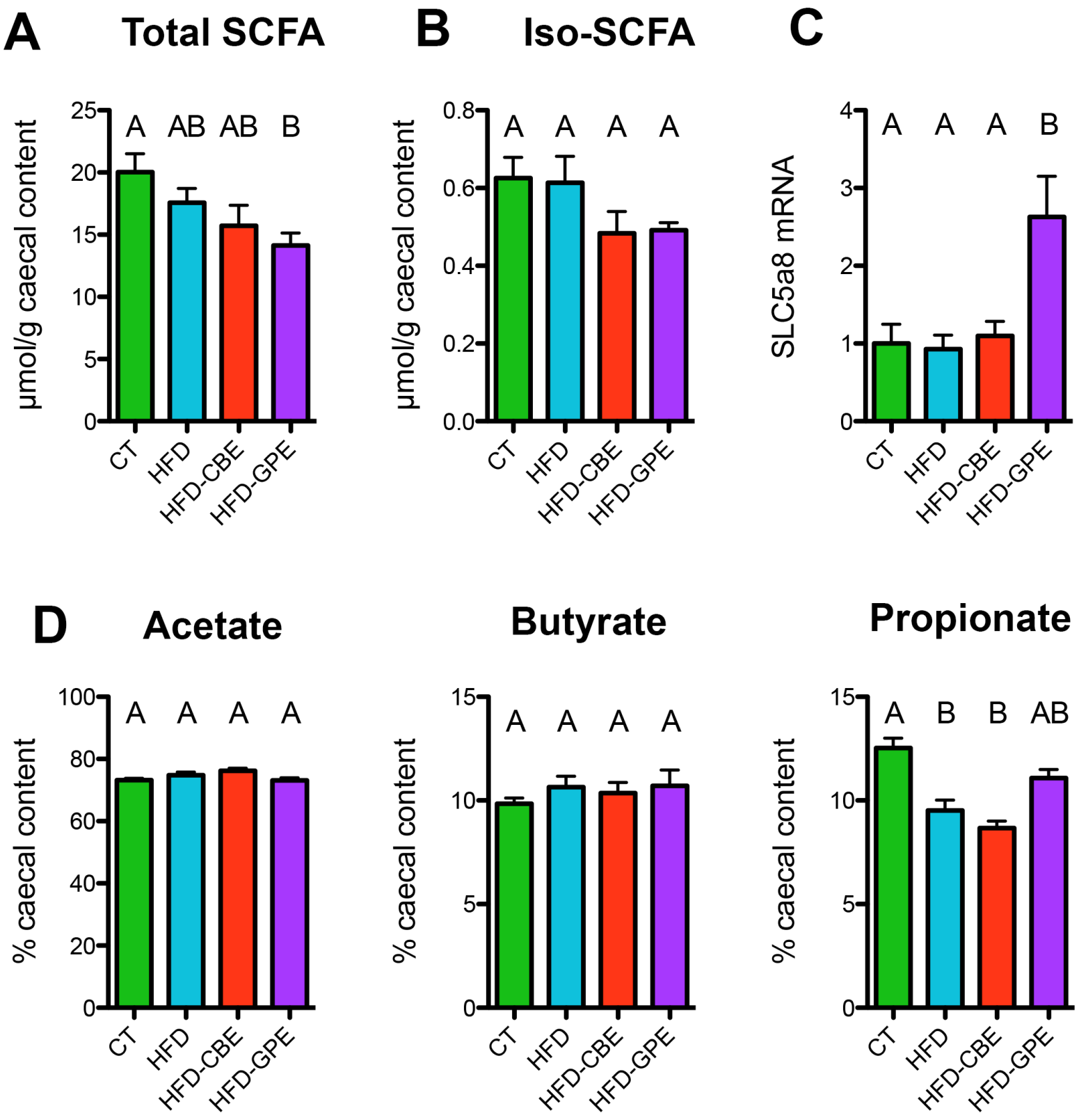

Primers	Forward Sequence	Reverse Sequence
Rpl19	GAAGGTCAAAGGGAATGTGTTCA	CCTGTTGCTCACTTGT
Cd11c	ACGTCAGTACAAGGAGATGTTGGA	ATCCTATTGCAGAATGCTTCTTTACC
Mcp1	GCAGTTAACGCCCCACTCA	CCCAGCCTACTCATTGGGATCA
Lbp	GTCCTGGGAATCTGTCCTTG	CCGGTAACCTTGCTGTTGTT
Cd68	CTTCCCACAGGCAGCACAG	AATGATGAGAGGCAGCAAGAGG
F4/80	TGACAACCAGACGGCTTGTG	GCAGGCGAGGAAAAGATAGTGT
Reg3g	TTCCTGTCCTCCATGATCAAA	CATCCACCTCTGTTGGGTTC
Intectin	GTTGCCCCTGATTCTGCTGG	GCACTATTGCAGAGGTCC-GT
ZO-1	TTTTTGACAGGGGGAGTGG	TGCTGCAGAGGTCAAAGTTCAAG
Occludin	ATGTCCGGCCGATGCTCTC	TTTGGCTGCTCTTGGGTCTGTAT
Claudin3	TCATCGGCAGCAGCATCATCAC	ACGATGGTGATCTTGGCCTTGG
Lyz1	GCCAAGGTCTACAATCGTTGTGAGTTG	CAGTCAGCCAGCTTGACACCACG
Ang 4	CTCTGGCTCAGAATGTAAGGTACGA	GAAATCTTTAAAGGCTCGGTACCC
Muc2	ATGCCCACCTCCTCAAAGAC	GTAGTTTCCGTTGGAACAGTGAA
Klf4	AGAGGAGCCCAAGCCAAAGAGG	CCACAGCCGTCCCAGTCACAGT
Proglucagon	TGGCAGCACGCCCTTC	GCGCTTCTGTCTGGGA
CYP7a1	GGGATTGCTGTGGTAGTGAGC	GGTATGGAATCAACCCGTTGTC
CYP7b1	TAGGCATGACGATCCTGAAA	TCTCTGGTGAAGTGGACTGAAA
CYP8a1	GATCCGTCGCGGAGATAAGG	CGGGTTGAGGAACCGATCAT
CYP27a1	TCTGGCTACCTGCACTTCCT	GTGTGTTGGATGTCGTGTCC
FXR	TGGGTACCAGGGAGAGACTG	GTGAGCGCGTTGTAGTGGTA
FGFR4	CTCGATCCGCTTTGGGAATTC	CAGGTCTGCCAAATCCTTGTC
FGF15	GAGGACCAAAACGAACGAAATT	ACGTCCTTGATGGCAATCG
SGLT1	TCTGTAGTGGCAAGGGGAAG	ACAGGGCTTCTGTGTCTTGG
GLUT2	CTGGGTCTGCAATTTTGTCA	TGTAAACAGGGTGAAGACCA
LFABP	ACCTCATCCAGAAAGGGAAGG	ACAATGTCGCCCAATGTCATG
CD36	GCCAAGCTATTGCGACATGA	ATCTCAATGTCCGAGACTTTTCAAC
SLC5a8	GCATATTCGGCATGGTTGGT	GGGCTCCAATTCCTACCCAT

Table 2. Concentrations of the main components of grape pomace extract and cinnamon extract.

Main tanin concentrations in GPE (mg/g of the extract)		
	mg/g of the extract	**Daily dose (ng/d)**
Catechin	1.732 ± 0.089	48,40 ± 3,23
Procyanidin B1 dimer	0.100 ± 0.011	2,79 ± 0,18
Procyanidin B2 dimer	0.311 ± 0.032	8,69 ± 0,58
Procyanidin B3 dimer	0.350 ± 0.022	9,78 ± 0,65
Procyanidin B4 dimer	0.090 ± 0.001	2,51 ± 0,16
Procyanidin C2 trimer	0.071 ± 0.001	1,98 ± 0,13
Epicatechin	1.011 ± 0.045	28,25 ± 1,88
Total tanins	3.66 ± 0.625	102,27 ± 6,83
Main anthocyanins concentrations in GPE		
	mg/g of the extract	**Daily dose (ng/d)**
Delphinidin-3-O-glucoside	1.635 ± 0.016	45,69 ± 3,05
Cyanidin-3-O-glucoside	0.513 ± 0.007	14,33 ± 0,95
Petunidin-3-O-glucoside	2.744 ± 0.027	76,67 ± 5,12
Peonidin-3-O-glucoside	8.687 ± 0.258	242,74 ± 16,21
Malvidin-3-O-glucoside	21.594 ± 0.213	603,39 ± 40,3
Peonidin-3-O-(6" acetyl-glucoside)	0.546 ± 0.003	15,26 ± 1,02
Malvidin-3-O-(6" acetyl-glucoside)	1.476 ± 0.026	41,24 ± 2,75
Peonidin-3-O-(6''-p-coumaryl-glucoside)	1.596 ± 0.018	44,6 ± 2,98
Malvidin-3-O-(6''-p-coumaryl-glucoside)	4.624 ± 0.012	129,21 ± 8,63
Total anthocyanins	43.416 ± 6.793	1213,15 ± 81,03
Phenolic composition of GPE		
	mg/g of the extract	**Daily dose (ng/d)**
Total phenolics (1)	82.663 ± 2.534	2309,81 ± 154,28
Total anthocyanins (2)	43.969 ± 3.497	1228,6 ± 82,06
Total tanins (3)	26.006 ± 1.066	726,67 ± 48,54

(1) Total phenolics, mg/g as gallic acid equivalent (Folin Ciocaleau assay)
(2) Total anthocyanins, mg/g as cyanidin-3-O- glucoside equivalent
(3) Total tanins, mg/g as procyanidin B2 equivalent (Bate-Smith assay)

Main components in CBE		
	mg/g of the extract	**Daily dose (ng/d)**
Total polyphenols	79	1174,45 ± 40,46
Proanthocyanidin A	90	1337,99 ± 46,09
Coumarin	9	133,8 ± 4,609
Cinnamaldehyde	1,8	26,76 ± 0,92
Eucalyptol	not detected	